Missouri S&T Library and Learning Resources

Scholars' Mine

Masters Theses

Student Theses and Dissertations

Summer 2017

Processing, microstructure, and properties of engineered diboride structures

Connor Charles Wittmaier

Follow this and additional works at: https://scholarsmine.mst.edu/masters_theses

 Part of the Ceramic Materials Commons

Department:

Recommended Citation

Wittmaier, Connor Charles, "Processing, microstructure, and properties of engineered diboride structures" (2017). *Masters Theses*. 7678.
https://scholarsmine.mst.edu/masters_theses/7678

This thesis is brought to you by Scholars' Mine, a service of the Missouri S&T Library and Learning Resources. This work is protected by U. S. Copyright Law. Unauthorized use including reproduction for redistribution requires the permission of the copyright holder. For more information, please contact scholarsmine@mst.edu.

PROCESSING, MICROSTRUCTURE, AND PROPERTIES OF ENGINEERED DIBORIDE STRUCTURES

By

CONNOR CHARLES WITTMAIER

A THESIS

Presented to the Faculty of the Graduate School of the

MISSOURI UNIVERSITY OF SCIENCE AND TECHNOLOGY

In Partial Fulfillment of the Requirements for the Degree

MASTER OF SCIENCE

IN

CERAMIC ENGINEERING

2017

Approved by

William G. Fahrenholtz, Advisor

Greg E. Hilmas

Jeremy Watts

PUBLICATION THESIS OPTION

This thesis has been prepared using the publication option, with the following sections made for submission and publication in peer review journals.

Paper I: Pages 16-30 are intended for submission to the Journal of the American Ceramic Society

Paper II: Pages 31-52 are intended for submission to the Journal of the American Ceramic Society

ABSTRACT

The mechanical properties and processing parameters of boride ceramics in foam and laminate architectures were evaluated. The ceramic reticulated foam was produced through a polymer substrate replication technique and the hardness and compressive strength were tested. The laminate structure was tested to evaluate the flexure strength and work of fracture as a function of temperature.

The foam architecture was produced using a TiB_2 slurry coating on a polyurethane reticulated foam preform. Foams sintered to 2150°C displayed an average grain size of 8.9 ± 7.3 μm, and a hardness of 17.3 ± 2.4 GPa. Crush testing foams were sintered at 1975°C, and displayed a specific strength of 208 ± 63 kPa with an overall porosity of 97%. For these specimens, it is likely that microcracking lowered the hardness, but the overall strength was controlled by the bulk density.

The laminate structures were fabricated using alternating layers of ZrB_2 and C–10 vol% ZrB_2. The structures were fabricated through the shaping of ceramic loaded thermoplastic polymers that underwent burnout and hot pressing cycles. These specimens had strong phase ZrB_2 layers that were about 150 μm thick alternating with weak phase layers that were about 20 μm thick. Specimens exhibited a maximum flexure strength of 311 ± 10 MPa at 1600°C, and an increased work of fracture compared to conventional ZrB_2 ceramics. The maximum fraction of inelastic work of fracture occurred at room temperature, and decreased as temperature increased. This was reflected in the length of the crack path through the specimen. Deflected cracks travelled through the center of the C–ZrB_2 layers in the material in Mode II fracture.

ACKNOWLEDGMENTS

I would like to thank my advisors, Dr. William Fahrenholtz and Dr. Gregory Hilmas for guiding my research throughout my research. Beyond offering their support and advice as my studies progressed, they offered me the chance to present my work before colleagues throughout the international community of materials scientists and engineers. I would also like to thank Dr. Jeremy Watts, who beyond being the final member on my committee has been extremely helpful and informative on many of the practical considerations of various experiments and procedures.

I would also like to acknowledge the Air Force Office of Scientific Research for providing partial funding for my degree. In particular, I would like to thank Dr. Ali Sayir who was the program director for the grant that funded my project, FA9550-14-1-0385.

Next, I would like to thank the UHTC research group for many interesting and sometimes informative conversations. They helped to expand my understanding of many fields of ceramics processing and properties, and many more that had only tangential relations to materials science at all. They made my experience and time in the lab much more entertaining and enjoyable.

Finally, I would like to thank my friends and family, for helping and supporting me at every step along the way. Without them, there is no doubt that I would not have made it to where I am now.

TABLE OF CONTENTS

LIST OF ILLUSTRATIONS

Page

Section

LIST OF TABLES

Page

Paper II

1. INTRODUCTION

The focus of this thesis is on the processing and properties of different structures made of diboride ceramics. Transition metal diborides are a group of materials that has received a great deal of interest in recent years. These materials are characterized by their high melting temperature and their strength, but they also display exemplary hardness as well as thermal and electrical conductivity.[1] This combination of properties has led to studies into the potential to use these materials for high temperature applications such as wing leading edges on hypersonic aircraft that require some degree of stiffness.[2, 3]

Two diboride materials in particular are of interest to this study, titanium diboride (TiB_2) and zirconium diboride (ZrB_2). For TiB_2, the most significant attribute is its high hardness value. While the exact number for the hardness of TiB_2 is debated across different studies, the majority of studies place the value around 25 GPa.[2, 4, 5] TiB_2 is also considered a high strength material, with a reported value of about 550 MPa at room temperature.[6] TiB_2 also exhibits a high melting temperature (~3225°C)[7], which makes it useful in high temperature applications, such as tools in contact with molten metal or as cutting tool materials.

The TiB_2 materials were used to make reticulated foam structures. The large amount of porosity in a foam specimen gives them an unusual combination of properties.[8] The porosity throughout the specimen leads to a high level of surface area per gram of material. This property lends itself to uses as a catalyst materials, where the larger surface area helps to speed up the rate of reactions.[9] Because the foam is reticulated the porosity is almost entirely interconnected and open to the surrounding environment, allowing

fluids to pass entirely through the material. By controlling the size of the porosity in the foam structure, it is possible to use a reticulated foam structure to filter the fluid that flows through.[10] Reticulated foams also retain a degree of strength and stiffness of the homogenous monolithic specimens of their constituent materials, allowing for their use as structural components.[11]

ZrB_2 has also been studied as a high temperature structural material. With a melting point of ~3250°C, ZrB_2 also has a high thermal and electrical conductivity.[1] This combination of properties makes this material highly suited to applications such as leading edges on hypersonic aircraft.[12] However, this material has a fracture toughness of 3.5 MPa$\sqrt{m}$[13] and it also displays significant oxidation when under atmospheric conditions at elevated temperatures, leading to studies of this material as part of composite systems.[14]

The ZrB_2 materials were used to make a laminate structure. These composites exhibit alternating layers of different material.[15] A few different varieties of laminates have been studied, including those with alternating layers of materials with different strength, levels of porosity, or materials under different stress states.[16, 17, 18] The goal for each of these structures is to increase the toughness of the final part, and thereby make the piece less sensitive to the flaws in a stressed section.[15] In these composites, the toughness is increased through either arresting cracks or deflecting them along one of the phases.[19] Either of these outcomes increases the fracture toughness as well as the work required to propagate a crack through a specimen.

The research presented in this thesis looked at the procedures for processing TiB_2 foams as well as ZrB_2 laminates. For both types of structures, this study focused on the

two topics of processing and mechanical properties. For the foams, the replication technique was used to replicate a polyurethane preform and the sintered foams were tested in uniaxial compression. For the laminate structures, ceramic loaded thermoplastic polymers were used to form the structure, and specimens were machined into bars which were tested in 4-point bending over a range of temperatures.

In pursuit of these studies, there are a few primary goals for this project to achieve. These are structured as the questions below:

1) Can a TiB_2 foam that retains a high intrinsic hardness be produced? What strength values would this structure exhibit?
2) Will a laminate of ZrB_2/ C-10 vol% ZrB_2 deflect cracks at room temperature and high temperatures? What is the work of fracture for specimens that do deflect cracks?
3) How do the ZrB_2/ C-10 vol% ZrB_2 laminates fail, and do they exhibit similar strength to homogenous ZrB_2 at all temperatures?

2. LITERATURE REVIEW

2.1 LATTICE STRUCTURE

Many transition metal diborides exhibit the P 6/mmm space group, giving the materials anisotropic intrinsic properties.[20] In this structure, there are alternating planes of metal and boron, as shown in Figure 2.1, where the transition metal planes are arranged in a hexagonally close packed structure and the boron plane is arranged in 6-member rings similar to graphite. This structure gives boron atoms 3 neighboring boron atoms and 6 transition metal atoms, while the transition metal atoms have 6 neighboring transition metal atoms and 12 neighboring boron atoms.

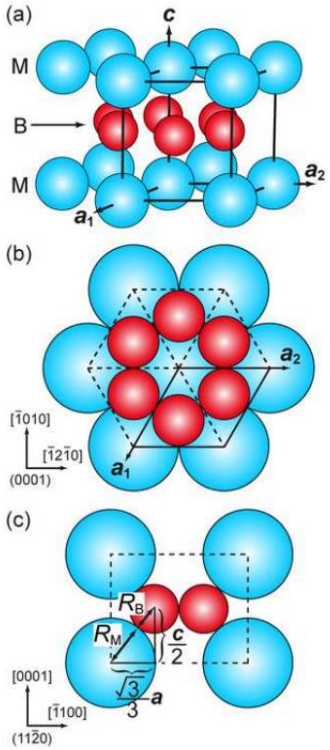

Figure 2.1. Representation of the hexagonal crystal structure of typical transition metal diboride from various perspectives. The solid lines in images (a) and (b) outline a unit cell[20]

Unit cells in these materials consist of a single formula unit. The dimensions of these unit cells are controlled by the length of the bonds between the transition metal atoms for the a-direction, and the transition metal-to-boron bonds control the length along the c-axis. The lattice parameters for TiB_2 are a = 3.04 Å and c = 3.24 Å. For ZrB_2 the lattice parameters are slightly smaller at a = 3.13 Å and c = 3.53 Å.[20]

The melting temperature of transition metal diborides is controlled by the strength of the bonds between transition metal atoms and boron.[1] The predicted melting temperature values for a majority of transition metal diborides are above 3000°C.[1] For these structures, it is generally accepted that the bonding among transition metal atoms is metallic, while bonds among boron atoms are covalent, and bonds between the transition metal and the boron is a mixture between ionic and covalent.[21] Because of the shared valence electrons in the metallic bonds among the transition metal atoms, these materials exhibit higher thermal and electrical conductivities along the a-axis than along the c-axis.

2.2 DENSIFICATION

Transition metal diborides in general, and TiB_2 in particular, are difficult to densify. One contribution to this is that the titanium diboride readily reacts with oxygen at temperatures below 1000°C.[22, 23]As this system is brought to higher temperatures, the oxide phases tend to promote grain coarsening, leaving entrapped porosity within the grains.[24] In testing this, several studies on the densification of TiB_2 have been performed, with the resulting materials reaching densities in excess of 95%.[4, 24, 25, 26]

Additionally, TiB_2 is typically densified while under pressure, using techniques such as hot pressing, hot isostatic pressing, or field assisted sintering.[6] The pressure is applied in these processes in order to promote densification processes. This effectively

means that the piece does not have to be at the sintering temperature for as long a time, which helps to limit the amount of grain growth that can occur. In hot pressing, the conditions required to achieve full density are typically reported to be around 32 MPa and up to 1900°C or above.[4, 6, 26] Conditions for sintering pressurelessly have also been reported, although they usually require sintering aids or higher temperatures to reach high densities.[24, 25]

Another common practice for densifying TiB_2 is to introduce a transition metal as an additive to form a liquid phase in the matrix at high temperature.[25, 27, 28] This allows for increased diffusion across the grain boundaries, thereby allowing materials to sinter to full density at a reduced temperature and pressure. There are a number of different additives that are commonly used, including iron, nickel, and cobalt.[25, 27] While these materials will help to densify the part, some of them reduce the strength and hardness of the final piece, especially at high temperatures (>1800°C).[25] Several additives, including silicon nitride, have been used to assist densification with a minimal impact on the strength of the specimens at low temperatures.[26, 29] These materials are reported to form a liquid phase during sintering, like the metallic additives, while also removing oxygen from the titanium within the material as the oxygen preferentially bonds with the silicon.[29]

With behavior similar to TiB_2 in oxidizing environments, ZrB_2 starts to react with the ambient atmosphere at around 1100°C.[30] This leads to an accumulation of oxygen within the material, and at elevated temperatures the oxide phases turn to liquid and enhance grain growth. Entrapped porosity and coarse grains are likely to be results of the presence of oxides.[1]

In many studies, ZrB_2 is fabricated through hot pressing, hot isostatic pressing, or field assisted sintering, as opposed to pressureless methods.[1] As with TiB_2, these pressure assisted processes serve to reduce the time and temperature required for sintering. ZrB_2 has been sintered over a range of temperatures, but generally it is reported that a pressure of 32 MPa and a temperature of 2100°C or greater are necessary for pure ZrB_2.[13, 31]

Additionally, additives have been used in ZrB_2 in order to aid in achieving full density. Several materials are commonly added to assist in sintering, and they may be split up into groups by the role that they play in the densification process. Some additives form a liquid phase in the structure and act to reduce the energy required for densifying processes, and these include materials such as silicon nitride.[32] The second category of materials react with the oxygen that is incorporated into the matrix causing the resulting oxide phases to leave the system in the form of a gas. These materials include boron carbide, carbon, and tungsten carbide.[33, 34, 35] It has been noted that with the addition of 8 wt% tungsten carbide, the required sintering temperature to densify ZrB_2 through hot pressing decreases to 1900°C.[1]

2.3 MECHANICAL PROPERTIES

2.3.1 Titanium Diboride. Titanium diboride (TiB_2) is a member of the group IV transition metals, and is perhaps best known for its high hardness. While the exact value for the intrinsic hardness of this material is debated, it has been shown in studies to be between 25 and 35 GPa.[2, 4, 5] This high level of hardness has contributed to this material being used in cutting applications, where the amount of wear on cutting surfaces is reduced by the mechanical properties. To this purpose, it is common to coat TiB_2 onto a metallic substrate, or to add this as a particulate component in a metallic matrix.[2]

The strength of TiB_2 has also been studied. For nominally pure TiB_2, it is reported that the strength will be around 500 MPa when the grain size is around 6 μm and the density is above 95% of the theoretical value.[6, 28] Increasing the density up to ~98% can yield specimens with a strength around 550 MPa.[6] The reported strength can change significantly depending on the additives used. Using less than 2 wt% metallic additives, flexure strengths up to ~700 MPa have been reported.[2] Non-metallic additives have also been used to help densify this material. There are a wide variety of these that have been reported, generally in the nitride and carbide groups, with some of the more effective additives including silicon carbide, silicon nitride, and aluminum nitride.[29] For these additives, a greater amount of dopant is required to produce dense TiB_2 as compared to the metallic additives.[2]

Another important mechanical property of TiB_2 is its fracture toughness. Generally, the fracture toughness measured for TiB_2 is reported as somewhere between 2 and 6 MPa√m, depending on the grain size and amount of secondary phase present in the matrix.[4, 26] Combined with the fact that the material does not display any significant R-curve behavior, this is one characteristic that limits the widespread application of TiB_2 as a structural material.[28]

2.3.2 Zirconium Diboride. Due to the high melting temperature of ZrB_2 (3250°C), and its high temperature properties, this material has received interest for use as structural parts in extreme environments. ZrB_2 has been proposed to be a suitable material for molten metal filters, catalyst support structures, cutting tools, and leading edges on hypersonic vehicles.[12, 36, 37] In all of these applications, it is important that the chosen material displays a degree of strength, tolerance for high temperature conditions,

and for some of these applications it is important for the material to be thermally or electrically conductive.

Due to the common requirements of the potential applications, the strength of ZrB_2, especially at high temperatures, is one of its most studied attributes. This material has been tested over a range of different temperatures, from room temperature all the way up to 2300°C.[31] At room temperature and under normal atmospheric conditions, the strength of ZrB_2 has been reported to be as high as 500 MPa.[30, 38, 39] These materials had density values above 95%, and were nominally pure specimens. The strength of ZrB_2 also shows a strong dependence on the temperature at which a specimen is tested. Neuman et al. performed testing over a range of different temperatures, from room temperature up to 2300°C in different ambient environments. From this series of tests, it was seen that nominally pure ZrB_2 exhibits a strength of approximately 380 MPa at room temperature, and maintains a strength of over 200 MPa from 1600°C up to the final testing temperature of 2300°C. In order to ensure that specimens tested at elevated temperatures were not affected by creep, flexure tests at high temperatures were performed using faster loading rates.

ZrB_2 also displays moderate hardness (15-23 GPa) and high elastic modulus (526 GPa) values when tested at room temperature.[1, 20, 40] While there have not been many tests of the hardness of ZrB_2 at elevated temperatures, the elastic modulus has been examined. In Neuman's study, the elastic modulus of specimens heated in air was tested using the static bend test. These specimens show an elastic modulus of 524 GPa at room temperature, decreasing linearly to ~370 GPa at 1300°C. Further increasing the temperature led to a steeper decrease in elasticity down to ~260 GPa at 1600°C. Other

studies have noted these decreasing trends in mechanical properties as a function of temperature, and the change in behavior at 1300°C has been attributed to the softening of grain boundaries or secondary phases.[41]

2.4 FOAMS

Foams are three dimensional structures that are characterized by high levels of porosity.[42, 43, 44, 45] These structures can be found in many places, from nature in the form of sponges and other natural cellular materials, to modern day packaging and insulation. There are also metal foams which can be used as a catalyst or a low density structural material as well as ceramic foams which have often been used as molten metal filters, catalysts, and reinforcing phases in composite materials.[46, 47, 48] The particular uses for each variety of foam can necessitate different structures.

There are two different primary structures of foams, reticulated and non-reticulated (or closed pore). Reticulated foams are characterized by their interconnected porosity, where the entire piece has all of its porosity open and the solid structure exists as a series of struts.[11, 49] This type of structure allows fluids to flow through the piece, leading to its common use as a filter catalyst, or as a scaffold for bioactive applications.[9, 50, 51] It is also possible to fill in all of the porosity in this type of specimen with a different material. This property is commonly used to produce composites that use the foam structure as a reinforcing phase, lending either stiffness or hardness to the structure, or possibly reducing the bulk density.[47, 52] Foams with closed pores also see a wide range of applications. These foams may be readily used as a thermally insulating phase due to the limited heat conduction through the material.[11, 53, 54]

There are a variety of techniques to produce the different foam structures as ceramic materials, though they may be sorted into a few general categories. Foams may be made through the bubbling and solidification of a slurry or ceramic containing polymer (foaming), the use of a ceramic slurry to coat a pre-existing foam structure (the replication method), or the direct fabrication of a foam structure through selective deposition of a ceramic phase (as in 3D printing).[43, 45, 55]

The process of foaming is relatively simple, with the main step in the process being the formation of bubbles in a liquid gel or sol. This method is commonly used for making foams from materials such as polyurethane or cellulose.[56] In most cases this tends to produce foams with closed cells, but if the gas used to form the pores is flammable then it is possible to 'burn out' the thin walls that separate the pores, leaving a reticulated structure.

Replication is a common process to produce reticulated foam structures using a pre-existing foam substrate.[43, 44] This technique requires that a preform be coated by a slurry, depositing material on the substrate to create a mechanically sound foam. The preform used is commonly a polymer material (like polyurethane) because such materials can be burned out of the system in the final steps, leaving just the coating material.

Direct fabrication of foam structures is a relatively new approach.[57, 58] This method has been used to produce scaffold shapes for bioactive materials among other things, as it allows foams with specific engineered geometries to be fabricated.[59] This process uses a slurry or precursor material and deposits it onto a plate or other flat surface in a specified pattern, building up the structure layer by layer until the final part is built. Depending on the method, the next step may be to remove a binder or polymer phase as

in the coating process or to react a deposited precursor with the binder system to form the desired ceramic phase. In either case, the control over the geometry used in this method allows for a greater level of precision when analyzing behavior than other methods which rely on random orientations of foam.[60]

Because of their high level of porosity, foams and other cellular materials can display unusual behavior when undergoing mechanical testing.[8, 44, 61] The common method for determining the strength of foams is crush testing, where the foam is loaded in compression along one axis.[42] While foams with large strut sizes and higher bulk densities may undergo critical fracture in a method similar to dense ceramics, other foams with smaller struts and higher porosities exhibit gradual failure as the foam collapses in on itself.[49, 62] This gradual failure occurs as individual struts or small groups alternately load and break across the foam. When these struts break, they have a tendency to collapse into the remaining foam structure, increasing its effective density. As the foam continues to undergo loading during the test, force is applied to a greater cross-sectional area of struts in the foam, increasing the maximum load that the foam can sustain. This effect was studied by Maiti, and it was determined that the apparent strength of the foam would continue to increase as a function of crosshead displacement up to a point where it would reach a plateau, as seen in Figure 2.2.[61]

2.5 LAMINATES

Laminated structures have been used to help mitigate the brittle fracture behavior of ceramics.[16] While most homogenous ceramics suffer brittle fracture, some composites using engineered architectures have been designed to support load after their initial failure.[30, 63, 64] Laminates belong in this class of materials, along with particulate

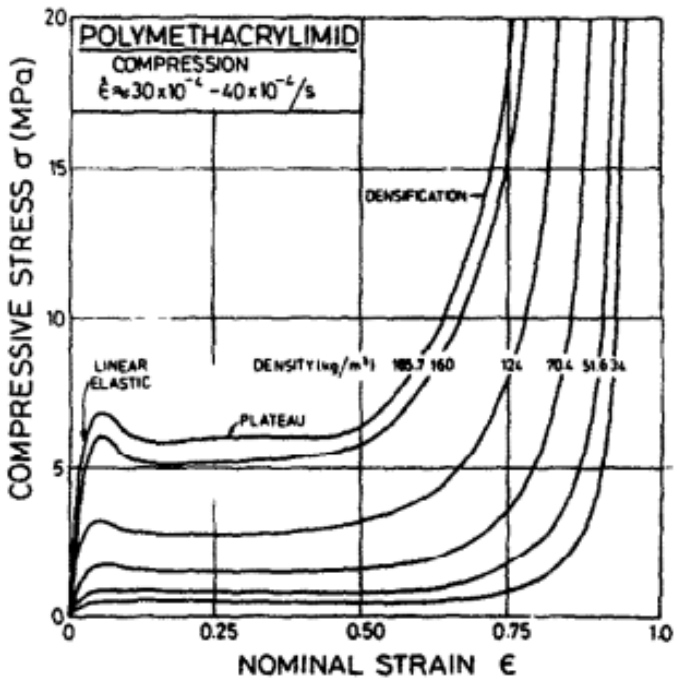

Figure 2.2. Compressive stress-strain curve for a brittle polymethacrylimid foam[61]

reinforced composites, chopped fibrous reinforced materials, and continuous fibrous monoliths. Of these materials, laminates tend to be some of the cheapest to produce and the fastest to manufacture.[65]

A large range of processing techniques exist for producing laminate structures.[15] Each of these processes have pros and cons, and in most cases the downsides have to do with the time required for fabrication or the complexity of the fabrication procedure.[65] A few notable methods that have been frequently used are alternating tape cast layers, slip coating on tape cast layers, and layers produced through plastic deformation of a ceramic embedded thermoplastic polymer.[16, 66]

The thermoplastic polymer method was originally used by Kovar et al. for the production of a fibrous monolithic material.[67] These materials make use of separate

polymer systems loaded with different phases of ceramics in order to build up the structure. Essentially, this process involves loading a weaker interface phase into one polymer system and the strong phase in another, then forming them in the green state, later removing the polymer and sintering them afterwards.[67, 68]

Several different varieties of laminates have been produced and tested, the primary differences between them being how the strong and weak phases are structured. These can be sorted into several different categories; whether the laminates rely on the difference in elastic modulus between materials or the residual stress caused by differences in thermal expansion between phases.[16, 17, 69]

For laminates that rely on a difference in elastic modulus between phases, the cracks will behave as described in models created by He and Hutchinson.[19] In order for impinging cracks from any possible angle to be deflected, the elastic modulus of the weaker phase must be a quarter or less than that of the other. Any deflection occurs because the energy required to extend the crack through the phase with high toughness is greater than the energy required for the crack to grow through the weaker phase along a non-optimal direction. This causes the crack to propagate parallel to the loading direction which takes a greater level of energy than travelling through the same material perpendicular to the loading axis, thereby increasing the amount of work necessary to fracture the part entirely.[65]

While the strength and work of fracture of laminated specimens are not intrinsic properties, they are commonly reported and allow for comparisons to be made to conventional ceramics. Clegg et al. saw increases of more than two orders of magnitude in the work of fracture for laminates over conventional ceramics.[66] The reduction in

strength for these materials was seen to be negligible, indicating that the structures tested did not affect the loads that the part could support when compared to conventional ceramic specimens of the same material.

Some laminates have been reported that rely on residual thermal stresses between layers in order to increase the work of fracture.[69] It is possible to see crack deflection in these specimens, but this doesn't occur as often as in laminates with alternating weak and strong layers. The study of these materials has shown that the composites see a ~70% reduction in strength when compared to the same material as a dense, conventional ceramic.[69]

PAPER

I. PROCESSING AND MECHANICAL PROPERTIES OF TiB_2 RETICULATED FOAMS

Connor C. Wittmaier and William G. Fahrenholtz
Missouri University of Science and Technology
Materials Science and Engineering Dept.
1400 N. Bishop Ave.
Rolla, MO 65409

ABSTRACT

Titanium diboride foams were produced using the foam replication method. Sintering conditions were determined by studying the densification behavior of pressed pellets. Sintering at 2150°C for 1 hour resulted in pellets that had a relative density of 95% with a hardness of 22.6 GPa, and a grain size of 1.3 μm. Foams sintered at 2150°C exhibited hardness values of 17.3 ± 2.4 GPa. Based on strength values that were lower than expected, as well as the appearance of the microstructure, microcracks are likely present in the sintered foams. Crush test specimens sintered at 2150°C had a strut density of 4.3 g/cm^3 (95% relative density) with an overall porosity of 97%. Foams sintered at 1975°C exhibited an average maximum compressive strength of 7.1 ± 2.2 kPa , with a compression modulus of 21 kPa. Based on these results, TiB_2 foams show promise as a reinforcing phase in applications where hardness and wear resistance need to be increased.

1. INTRODUCTION

Titanium diboride (TiB_2) has strong covalent bonding, a high melting temperature (3225 °C)[1], high elastic modulus (~580 GPa)[2, 3, 4], and high hardness (~32 GPa).[5] These properties make TiB_2 useful in applications ranging from cutting tools and wear resistant coatings to armor plates and crucibles.[4] Titanium diboride foams may be useful as lightweight structural materials, or as an interpenetrating phase that can increase hardness or wear resistance of other materials.[6, 7, 8, 9]

Numerous types of foams can be produced and they are categorized based on the geometry and interconnectivity of the porosity. One structure of particular interest is reticulated foams, which are co-continuous structures with continuous open porosity and a continuous network of struts of the solid material.[9, 10, 11] One process that can be used to produce reticulated foams is the foam replication method, which was popularized by Schwartzwalder and Somers.[12] Foam replication works by coating a ceramic slurry onto a polymer foam substrate that is later removed, leaving a skeleton of ceramic material.[11]

Foams have seen widespread use for their properties. They exhibit high specific surface area, and the size of the cells that make them up can be varied greatly.[13] These properties lead to a large array of uses, from packaging products made of polymer foams to catalytic substrates and filters for foams made from ceramic materials.[9, 14, 15] The density of foams can vary, yielding specimens with open porosities ranging from 75% to >90%.[11] Specimens produced by Jun et al. demonstrate specific strengths of 5.4 MPa for specimens of 7% relative bulk density as well as strengths ≥9.3 MPa with 9% relative bulk density.[16] One potential application for hard ceramic foams is as a reinforcing phase

in a metal matrix for abrasion resistant parts, such as brake pads or calipers.[17] These materials can also be used for making parts such as pistons or cylinder liners in engines.[18]

Because of their high melting point and low self-diffusion coefficient, TiB_2 and other transition metal diborides are difficult to densify without applied pressure.[24] TiB_2 has been shown to require temperatures above 2050°C in order to attain >95% of the theoretical density.[19] Additionally, TiB_2 readily oxidizes and the presence of surface oxide impurities inhibit densification by promoting grain coarsening at elevated temperatures.[19] Problems with densification can be mitigated through the use of sintering aids such as carbon, boron carbide, or silicon nitride that react with and remove oxides from particle surfaces.[19, 20, 21, 22] Using processes like hot pressing, along with sintering additives, can enhance densification so that near full density can be achieved at temperatures as low as 1700°C.[23] Some studies have reported densification of TiB_2 through pressureless sintering processes, and these typically require either temperatures over 2000°C or liquid phase sintering additives like nickel in addition to reducing additives like graphite.[19, 24]

The purpose of this study was to produce reticulated foams of TiB_2 and to test the properties. The foams underwent crush testing to determine their compressive strength, as well as indentation testing to determine the hardness of the struts.

2. EXPERIMENTAL PROCEDURE

The starting materials were commercially available TiB_2 (Treibacher Industrie AG, Althofen, Austria) and phenolic resin (GP 2074, Georgia Pacific Chemicals, Atlanta, GA; 41 wt% C yield after char). In order to determine appropriate slurry compositions,

suspension stability and solids loading tests were performed. For the suspension stability tests, 3 g of TiB_2 powder was put into a graduated cylinder along with 9 ml of methyl ethyl ketone (MEK) and then agitated in an ultrasonic bath for 5 min. For direct comparisons between conditions using different dispersant systems in different amounts. Two polymer dispersants (Dolapix CE-64, Zschimmer and Schwarz, Lahnstein, Germany; and Disperbyk-110, BYK Additives and Instruments, Wesel, Germany) with acidic end groups were used in the suspension stability tests. Levels of dispersants ranged from 0 to 2.5 mg/m^2 in increments of 0.5 mg/m^2. Powders were dispersed using ultrasonic agitation (), and then allowed to settle undisturbed for 5 days to observe the amount of powder that settled out of suspension. Evaluation of the stability of the suspensions was qualitative, with the most desirable conditions being those that resulted in the least amount of powder settling. The stability study showed that suspensions with no dispersant added were the most stable.

A second dispersion study performed was to determine the optimal solids loading, by maximizing the solids loading while maintaining a low enough viscosity to allow for coating on all internal surfaces of a reticulated foam substrate. Slurries were prepared using 20 g of MEK in a polyethylene milling jar and incrementally adding TiB_2 powder every 30 min. Mixtures were ball milled at 100 rpm in between additions. Qualitatively, the highest possible solids loading was approximately 28 vol% TiB_2.

To produce foams, powders were ball milled in batches of 80 g of TiB_2 powder using TiB_2 media in a high density polyethylene jar with 37 g of MEK. Batches were milled for 24 hours at ~100 rpm to break up agglomerates. After 24 hours, 2.95 g phenolic resin (2.5 wt% superaddition that should yield 1 wt% carbon) was added, and

the mixture was milled for another 2 hours to ensure the resin dissolved and was dispersed.

The slurry was dried by rotary evaporation at 70°C under a vacuum (~27kPa) (Rotavapor R-124, Buchi, Flawil, Switzerland). The dried powder was passed through a 60 mesh sieve to remove large agglomerates. Pellets were produced from the granulated powder by uniaxially pressing ~4 g of powder in a 1.3 cm diameter steel die under a pressure of ~77 MPa. Pellets were sintered under an argon atmosphere for one hour at temperatures ranging from 1800 to 2150°C. Before heating, the furnace was evacuated to ~15 Pa and backfilled with a gas mixture containing 90 vol% argon and 10 vol% hydrogen (Ar10H). The purging-backfilling process was repeated 4 times. Then, the furnace was evacuated to ~15 Pa and heated at a rate of ~10°C/min. Isothermal holds of 1.5 hour were performed at 1250°C and 1600°C under a vacuum, allowing the atmosphere to drop below 15 Pa. The holds were used to remove volatile species produced by decomposition of surface oxides and the length of the holds was determined by the time required for the furnace pressure to decrease to ~20 Pa. After the second isothermal hold, the furnace was backfilled with Ar10H to a nominal pressure of 10^5 Pa. The furnace was then heated to its target sintering temperature and held for 1 hour. Sintered pellets were cross sectioned and polished with successively finer diamond abrasives with a final size of 0.25 μm. Vickers indentation (Duramin 5, Struers, Cleveland, OH) with a load of 500 gf and a dwell time of 5 seconds was performed to determine the hardness of the specimens.

Polished cross sections were thermally etched for microstructure characterization. Specimens were heated under vacuum (~13.3 Pa) at a rate of 25°C to a temperature of

1400°C and held for 1 hour. The surfaces of the specimens were then observed using scanning electron microscopy (SEM; S4700, Hitachi, Tokyo, Japan) with an accelerating voltage of 5 kV. Grain sizes were estimated from SEM images using computerized image analysis (Image J, National Institutes of Health, Bethesda, MD). The average feret diameter was determined by measuring 300 grains.

The preforms used for replication were reticulated polyurethane foams with approximately 4 pores per cm. The pores were anisotropic, with a strut length of 3.2 ± 0.8 mm in the c direction and 1.7 ± 0.4 mm in the a and b directions. With a strut width of 0.17 ± 0.03 mm, the porosity in the foam was fully open. As a result, the TiB_2 slurry fully infiltrated the preforms and coated the struts with a uniform layer of ceramic particles. For coating, preforms were submerged in the ceramic slurry, squeezed to compress the submerged foam, and then allowed to relax to draw the slurry into the foam to coat the struts. Foams were then removed from the slurry and compressed to eliminate excess slurry from the open pores in the preform. The coating process was repeated for a second time, and the foams were dried in ambient laboratory conditions, which allowed the solvent to vaporize and left behind the polymer struts with a coating of powder on the outside.

Dried foams were heated in Ar10H to decompose the preform. The furnace was heated from room temperature to 600°C at a rate of 5°C/min. Isothermal holds that were two hours long were used at 260°C and 300°C to burnout the polymer preform. After burnout, a skeletal structure of unsintered TiB_2 powder was left in the form of the polymer structure. The foam was transferred into another furnace, and put through a

sintering cycle. This cycle was the same as described above for the pellets with final temperatures of either 1975°C or 2150°C.

Sintered foams were cut into cubes approximately 2.5 cm on each side. The cubes were tested in compression following ASTM C365 using an Instron (Model 5881, Instron, Norwood, MA) load frame, with a crosshead displacement rate of 0.5 mm/min. Specimens were compressed until the deflection was at least 10% of the specimen height, which was generally around 3 mm. A total of 5 foams sintered at 1975°C underwent crush testing in this study, while no foams sintered at 2150°C underwent crush testing.

Vickers hardness was measured for the TiB_2 struts in the foams, using an average of 10 indents at a load of 500 gf. Testing was accomplished by first infiltrating the foams with epoxy resin, cutting, and then polishing to a 0.25 μm finish. Microstructures of foam struts were also examined using SEM.

3. RESULTS AND DISCUSSION

Significant densification of TiB_2 pellets required temperatures of 2100°C or higher (Figure 1). Sintering at temperatures from 1800°C to 1950°C for 1 hour produced bulk densities of around 2.7 g/cm^3, which was ~60% relative density. These values were similar to the green density, which was 2.6 g/cm^3 or about 58% relative density. Increasing the sintering temperature to 2050°C resulted in an increased density of 3.06 g/cm^3, or about 68% relative density. Density increased more substantially when heating to 2100°C or higher where relative density increased to more than 90%. A maximum density of 4.3 g/cm^3 (~95%) was achieved at a sintering temperature of 2150°C. This

shows that in order to achieve relative densities above 90%, sintering temperatures of 2100°C or greater are required.

The densified TiB_2 pellets had defects along some grain boundaries, which are predominantly cracks or pores, as seen in Figure 2. The average grain size of pellets sintered at 2150°C was 1.3 ± 0.8 μm with a maximum grain size of ~5 μm. The defects had maximum widths of 0.1 ± 0.05 μm with the largest ones reaching ~0.5 μm. The measured hardness of the 95% dense TiB_2 pellets was 22.6 ± 1.5 GPa, which is lower than the intrinsic hardness value of fully densified TiB_2, which is ~32 GPa. Observation of the Vickers indentations on the surface of specimens showed that cracks tended to propagate preferentially through secondary phases and porosity.

The struts in foams displayed similar densification behavior to the pellets. Sintering at 1975°C resulted in a bulk density of 2.75 g/cm^3 in the struts and an overall bulk density for the foam of 0.16 g/cm^3. Based on the bulk density of the struts, they were ~61% dense after sintering at 1975°C, indicating that the struts should still contain open, interconnected porosity. This was confirmed by observation of the microstructures (Figure 3). Vickers indentation on the strut in a foam sintered at 1975°C showed the hardness was ~3 GPa, which was about the same as the hardness measured for pellets of similar bulk density.

Struts in foams sintered at 2150°C had bulk densities of 4.3 g/cm^3, which is about 95% relative density. The overall bulk densities of foams sintered at 2150°C were about 0.25 g/cm^3. The microstructure was examined by SEM as seen in Figure 4. The average grain size in the struts was 8.9 ± 7.3 μm. The larger grains in the struts are above the critical grain size that will cause microcracking in TiB_2, which is caused by the

anisotropic thermal expansion values in the hexagonal TiB_2 crystal structure.[25, 26] The hardness of the struts in foams sintered at 2150°C was 17.3 ± 2.4 GPa, which is lower than expected based on the accepted hardness of TiB_2 (~32 GPa) and the hardness measured for pellets in the present study that were sintered at the same temperature (22.6 ± 1.5 GPa). The lower hardness of the struts compared to the sintered pellets could be a result of the geometry of the specimen. More specifically, foam sections mounted in the epoxy resin could deform macroscopically under the indentation load. The polymeric resin supporting the struts has a lower elastic modulus than TiB_2, which would support the material in a dense ceramic. The reduced hardness could also be due to microcracking that would result from the larger average grain size of the struts.

Foams sintered at 1975°C exhibited two different regimes of crushing behavior (Figure 5). At low crosshead deflection (<4 mm), the crosshead came into contact with an increasing cross-sectional amount of material as deflection increased until a point (~4 mm extension) where the cross-sectional area of struts in contact with the platens was relatively constant. In the regime of increasing load, the foam exhibited a compressive modulus of ~21 kPa as the cross-sectional area of foam under load increased while in the constant load regime (>4 mm), the material displayed an average compressive strength of ~7.1 ± 2.2 kPa and a compressive modulus of ~5 kPa. The specific strength calculated here divided the average strength of the foam specimens by their relative density. In this regime, the top struts of the foam broke as other struts were loaded, yielding a net balance on the effective surface area under load. This behavior is consistent with previous reports and models of crush tests.[27, 28] Based on the analysis in those reports, the crush strength of the foams could be increased by increasing the strut thickness, which would provide

additional support for the struts through an increased size of ‘nodes’ where struts intersect.

4. CONCLUSIONS

TiB_2 foams were produced by the foam replication method and tested to determine the hardness, crush strength, and compressive modulus. A sintering study on TiB_2 pellets revealed that temperatures of 2100°C or higher were required for densification of TiB_2. The hardness of pellets densified at 2150°C was 22.6 ± 1.5 GPa and the average grain size was 1.3 µm. Foam specimens densified at 2150°C had a hardness of 17.3 ± 2.4 GPa and a grain size of 8.9 ± 7.3 µm, while foams densified at 1975°C had a hardness of ~3 GPa and particles exhibiting only partial necking. The foams sintered at 1975°C also showed a compressive strength of 7.1 kPa with a compression modulus of 21 kPa. TiB_2 foams were successfully produced and tested, showing promise for the use as a hard, reinforcing phase in composite materials or as a lightweight structural material.

REFERENCES

1. J. L. Murray, P. K. Liao, and K. E. Spear, "The B-Ti (Boron-Titanium) system," *Bulletin of Alloy Phase Diagrams,* 7[6] 550-55 (1986).
2. N. L. Okamoto, M. Kusakari, K. Tanaka, H. Inui, and S. Otani, "Anisotropic elastic constants and thermal expansivities in monocrystal CrB2, TiB2, and ZrB2," *Acta Materialia,* 58[1] 76-84 (2010).

3. J. Besson, F. Valin, P. Lointier, and M. Boncoeur, "Densification of titanium diboride by hot isostatic pressing and production of near-net-shape components," *Journal of Materials Engineering and Performance,* 1[5] 637-49 (1992).

4. R. G. Munro, "Material properties of titanium diboride," *Journal of Research of the National Institute of Standards and Technology,* 105[5] 709 (2000).

5. F. W. Vahldiek and S. A. Mersol, "Slip and microhardness of IVa to via refractory materials," *Journal of the Less Common Metals,* 55[2] 265-78 (1977).

6. D. Vallauri, I. C. Atías Adrián, and A. Chrysanthou, "TiC–TiB2 composites: A review of phase relationships, processing and properties," *Journal of the European Ceramic Society,* 28[8] 1697-713 (2008).

7. S. C. Tjong and K. C. Lau, "Abrasive wear behavior of TiB2 particle-reinforced copper matrix composites," *Materials Science and Engineering: A,* 282[1–2] 183-86 (2000).

8. L. Vazquez and J. M. Sanchez, "Influence of titanium diboride additions on the sintering behavior of nanoporous fumed silica composites," *Composites Part B: Engineering,* 90 416-23 (2016).

9. M. V. Twigg and J. T. Richardson, "Fundamentals and Applications of Structured Ceramic Foam Catalysts," *Industrial & Engineering Chemistry Research,* 46[12] 4166-77 (2007).

10. C. Voigt, T. Zienert, P. Schubert, C. G. Aneziris, and J. Hubálková, "Reticulated Porous Foam Ceramics with Different Surface Chemistries," *Journal of the American Ceramic Society,* 97[7] 2046-53 (2014).

11. U. F. Vogt, M. Gorbar, P. Dimopoulos-Eggenschwiler, A. Broenstrup, G. Wagner, and P. Colombo, "Improving the properties of ceramic foams by a vacuum infiltration process," *Journal of the European Ceramic Society,* 30[15] 3005-11 (2010).

12. S. Karl and A. V. Somers, "Method of making porous ceramic articles." in. Google Patents, #3090094. (May 21, 1963).

13. J. Luyten, I. Thijs, W. Vandermeulen, S. Mullens, B. Wallaeys, and R. Mortelmans, "Strong ceramic foams from polyurethane templates," *Advances in Applied Ceramics: Structural, Functional & Bioceramics,* 104[1] 4-8 (2005).

14. D. A. Heirschfeld, "Processing of Porous Oxide Ceramics," *Key Engineering Materials* 115 65-80 (1995).

15. M. Emmel, C. G. Aneziris, F. Sponza, S. Dudczig, and P. Colombo, "In situ spinel formation in Al_2O_3–MgO–C filter materials for steel melt filtration," *Ceramics International,* 40[8, Part B] 13507-13 (2014).

16. I.-K. Jun, Y.-M. Kong, S.-H. Lee, H.-E. Kim, H.-W. Kim, and K. C. Goretta, "Reinforcement of a Reticulated Porous Ceramic by a Novel Infiltration Technique," *Journal of the American Ceramic Society,* 89[7] 2317-19 (2006).

17. J. Liu, J. Wu, and J. Binner, "Cutting resistance of metal-ceramic interpenetrating composites," *Ceramics International,* 43[2] 2815-23 (2017).

18. T. Miyajima and Y. Iwai, "Effects of reinforcements on sliding wear behavior of aluminum matrix composites," *Wear,* 255[1–6] 606-16 (2003).

19. S. Baik and P. F. Becher, "Effect of Oxygen Contamination on Densification of TiB_2 " *Journal of the American Ceramic Society,* 70[8] 527-30 (1987).

20. J.-H. Park, Y.-H. Koh, H.-E. Kim, C. S. Hwang, and E. S. Kang, "Densification and Mechanical Properties of Titanium Diboride with Silicon Nitride as a Sintering Aid," *Journal of the American Ceramic Society,* 82[11] 3037-42 (1999).

21. S. Zhu, W. G. Fahrenholtz, G. E. Hilmas, and S. C. Zhang, "Pressureless Sintering of Zirconium Diboride Using Boron Carbide and Carbon Additions," *Journal of the American Ceramic Society,* 90[11] 3660-63 (2007).

22. S. C. Zhang, G. E. Hilmas, and W. G. Fahrenholtz, "Pressureless Densification of Zirconium Diboride with Boron Carbide Additions," *Journal of the American Ceramic Society,* 89[5] 1544-50 (2006).

23. E. Kang and C. Kim, "Improvements in mechanical properties of TiB_2 by the dispersion of B_4C particles," *J Mater Sci,* 25[1] 580-84 (1990).

24. M.-A. Einarsrud, E. Hagen, G. Pettersen, and T. Grande, "Pressureless Sintering of Titanium Diboride with Nickel, Nickel Boride, and Iron Additives," *Journal of the American Ceramic Society,* 80[12] 3013-20 (1997).

25. R. W. Rice and R. C. Pohanka, "Grain-Size Dependence of Spontaneous Cracking in Ceramics," *Journal of the American Ceramic Society,* 62[11-12] 559-63 (1979).

26. M. K. Ferber, P. F. Becher, and C. B. Finch, "Effect of Microstructure on the Properties of TiB2 Ceramics," *Journal of the American Ceramic Society,* 66[1] C-2-C-3 (1983).

27. H. I. Bakan and K. Korkmaz, "Synthesis and properties of metal matrix composite foams based on austenitic stainless steels –titanium carbonitrides," *Materials & Design,* 83 154-58 (2015).

28. S. K. Maiti, L. J. Gibson, and M. F. Ashby, "Deformation and energy absorption diagrams for cellular solids," *Acta Metallurgica,* 32[11] 1963-75 (1984).

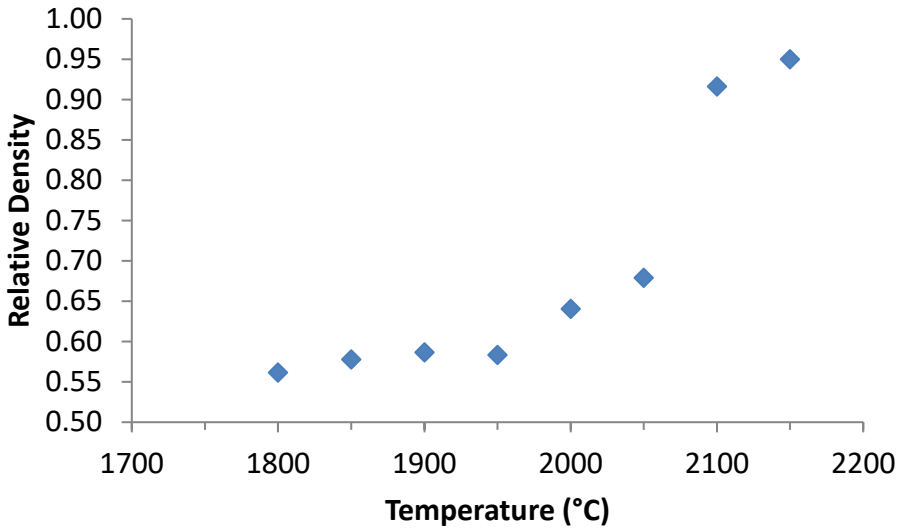

Figure 1. Relative densities of TiB_2 pellets as a function of sintering temperature.

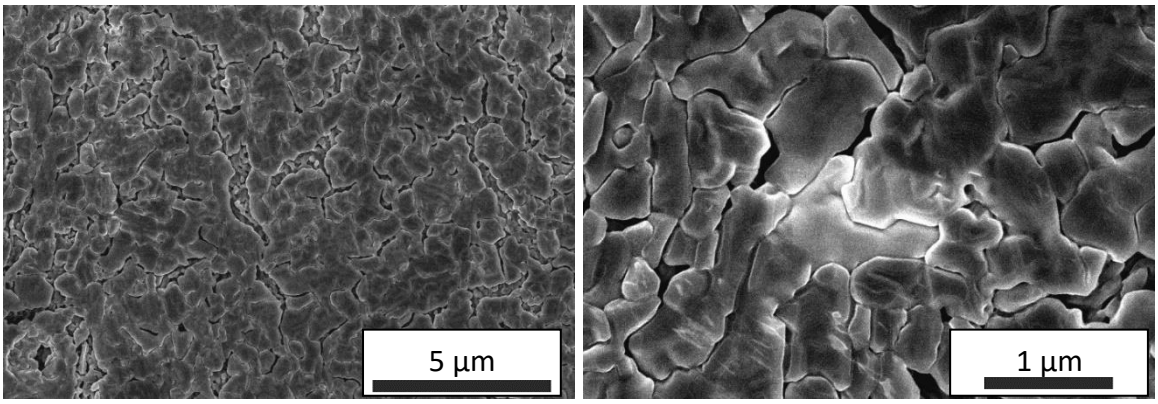

Figure 2. Microstructures of TiB_2 pellet sintered at 2150°C.

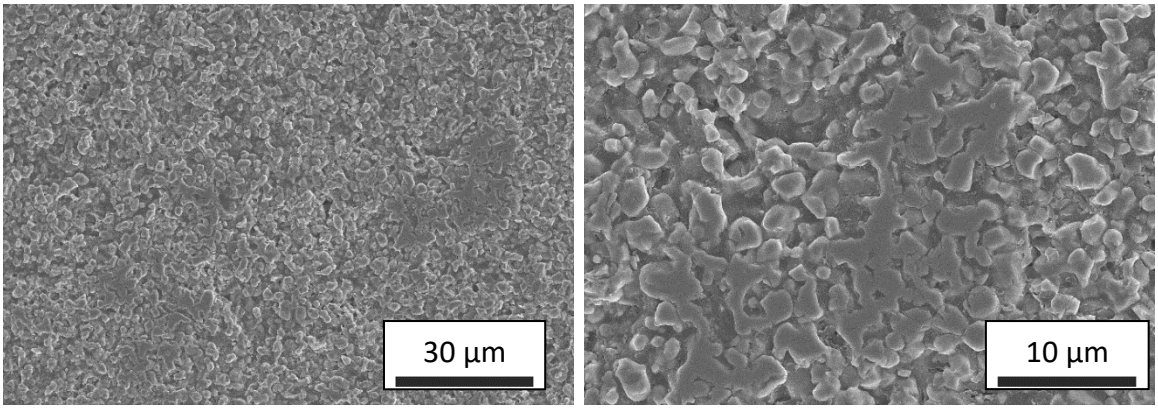

Figure 3. Microstructure of a strut of a TiB_2 foam sintered at 1975°C.

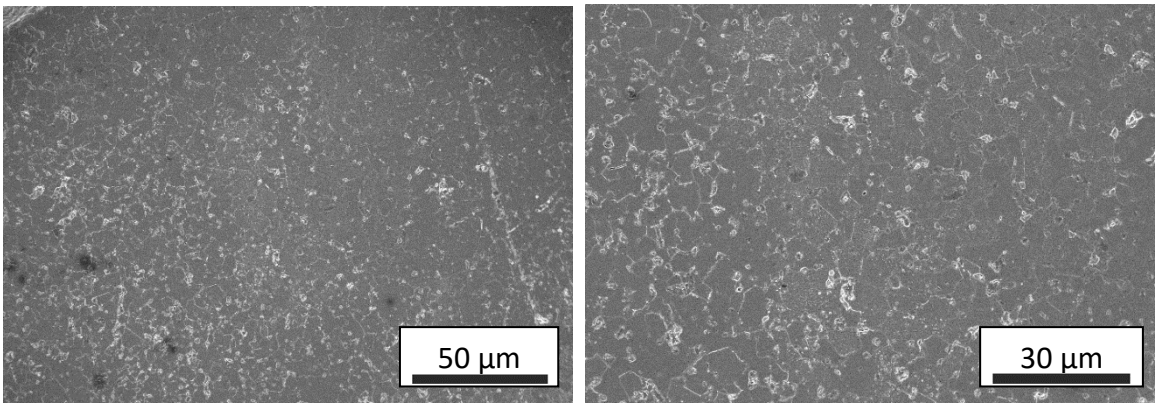

Figure 4. Microstructure of a strut of a TiB_2 foam sintered at 2150°C.

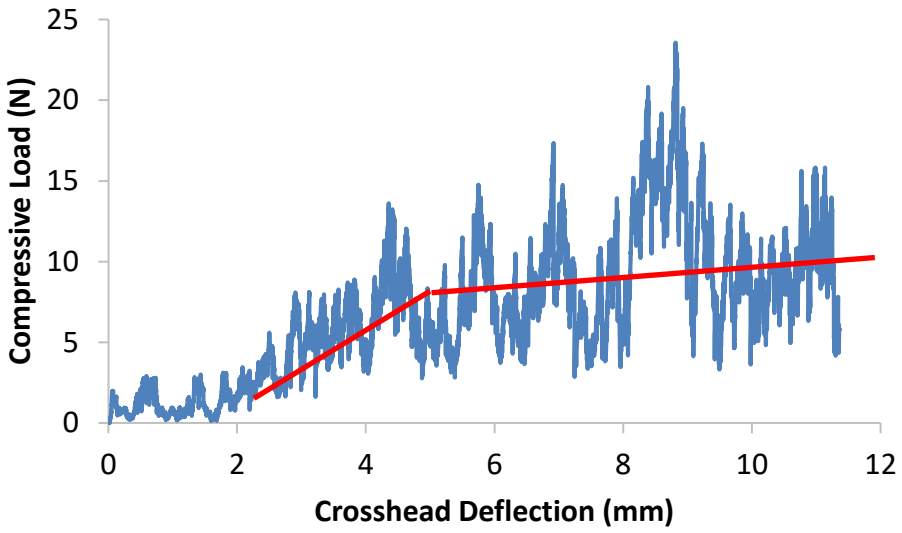

Figure 5. Load-Displacement curve for a TiB_2 foam sintered at 1975°C.

II. PROCESSING AND ELEVATED TEMPERATURE MECHANICAL PROPERTIES OF ZrB_2-BASED LAMINATES

Connor C. Wittmaier, William G. Fahrenholtz, Greg E. Hilmas
Missouri University of Science and Technology
Materials Science and Engineering Dept.
1400 N. Bishop Ave.
Rolla, MO 65409

ABSTRACT

Zirconium diboride-based laminates were produced by hot pressing preforms consisting of alternating layers of ZrB_2 and carbon + 10 vol % ZrB_2. Individual layers were produced by mixing the starting powders with thermoplastic polymers and pressing them into sheets. After binder removal, preforms were densified by hot pressing at 2050°C for 1 hour at a pressure of 32 MPa. Laminate samples had ZrB_2 layers ~150 μm thick and C-ZrB_2 phase layers ~20 μm thick. The flexure strength and work of fracture were measured over a range of temperatures, with a maximum strength of 311 ± 10 MPa at 1600°C and a maximum inelastic work of fracture of 1.3 ± 0.4 kJ/m^2 at 1400°C. Cracks were deflected by the weaker C-ZrB_2 layers, travelling along the center of the C-ZrB_2 layers over extended distances. Cross sectional images of the fracture surface of the specimens showed a greater amount crack travel parallel to the layers at room temperature, with decreasing crack propagation within the weak phase 2000°C. The work of fracture of tested laminates was greater at all temperatures than the work of fracture of conventional ceramic specimens.

1. INTRODUCTION

Zirconium diboride is a widely studied ultra-high temperature ceramic (UHTC) material. It has a high melting temperature (~3250°C)[1], along with high elastic modulus (~525 GPa) and strength (up to ~500 MPa for nominally pure ZrB_2 ceramics).[1, 2, 3, 4, 5] This combination of properties has led to potential applications including cutting tools, molten metal crucibles, and leading edges for hypersonic aerospace vehicles.[6, 7, 8] The mechanical properties of ZrB_2 have been studied at room temperature and elevated temperatures. As with most ceramics, zirconium diboride has relatively low fracture toughness (~3 MPa$\sqrt{m}$).[3, 5] One method commonly used to mitigate the low fracture toughness is to introduce second phases, as either a continuous secondary phase or as dispersed particulates.[9, 10]

Laminate structures have been shown to increase the damage tolerance of brittle materials by using alternating layers composed of materials with different properties. [11, 12, 13, 14] In particular, laminate structures exhibiting extensive crack deflection tend to incorporate layers of a weaker phase alternating with layers of a stronger phase. [11, 15, 16] Deflection occurs because the energy required to propagate a crack through the weaker phase is lower than propagating a crack through interfaces and into stronger phases. [16, 17] Conventional fracture toughness (i.e., K_{IC}) measurements do not capture the damage tolerance of laminates because fracture occurs in a mixture of modes.[18, 19] Quantifying the work of fracture can provide a more accurate measure of the damage tolerance since this measurement considers the total area under the load-deflection curve (i.e., the energy associated with fracturing the specimen regardless of fracture mode). For example, Clegg et al. reported that work of fracture increased by about 100-fold for a silicon carbide –

carbon laminate compared to a conventional silicon carbide ceramic.[20] Hence, laminates are a promising approach for increasing damage tolerance.

Several methods can be used to produce laminate structures including tape casting, centrifugal casting, and slip casting.[20, 21, 22, 23] For the present study, layers were produced by stacking and pressing sheets made from thermoplastic polymers that were loaded with ceramic powders. This process is based on the procedure described in a paper by Kovar et al. for producing textured materials using conventional powder processing routes.[24] The major advantage of this method is that it uses conventional ceramic powders rather than expensive high-strength fibers to increase damage tolerance. This method has been successfully used to produce fibrous monolithic structures with improved damage tolerance.[24]

The system used in this study consisted of alternating layers of ZrB_2 and C-10vol% ZrB_2. Graphitic carbon was chosen for the weak layer because of its low strength relative to the ZrB_2 as well as its chemical compatibility with ZrB_2. The phases in the laminate structure need to be inert with respect to each other to minimize interactions between layers (e.g., forming a diffusion zone that would prevent crack deflection). In this study, ZrB_2 was added to the graphite phase to improve the strength of the weak layer to maintain the strength of the overall laminate structure.

The purpose of the present study was to evaluate the mechanical properties of a zirconium diboride-based laminate architecture at room and elevated temperatures.

2. PROCEDURE

Each of the layers in the laminate was batched and prepared separately. For the weak layers, graphite (8.5 μm, Sigma Aldrich, St. Louis, USA) was attrition milled in acetone using spherical tungsten carbide – 6 wt% cobalt (WC-6Co) milling media in a Teflon coated mill jar for 2 hours to break up agglomerates and reduce the particle size. The resulting slurry was dried in a rotary evaporator at 70°C under a vacuum (~27kPa) (Rotavapor R-124, Buchi, Flawil, Switzerland). The dried powder was mixed with 10 vol% ZrB_2 (Grade B, HC Starck, Munich, Germany) by ball milling in acetone with WC-6Co in an HDPE jar then dried by rotary evaporation using the conditions described above. For the strong layers, ZrB_2 powder was batched with 2 vol% carbon black (Cabot 120, Cabot Corporation, Boston, USA) and 1.5 vol% boron carbide (B_4C) (Grade HD-20, HC Starck) to act as sintering aids. The powders were blended by ball milling in an HDPE jar for 2 hours in acetone with WC-6Co milling media and then dried by rotary evaporation using the conditions described above.

The powders prepared for each type of layer were individually mixed with a thermoplastic polymer (ethylene/ethyl acrylate MI-20, Dow Chemical Company, Midland, USA) in a high shear mixer (Rheocord System 40, Haake Buchler Instruments, Saddle Brook, USA) at 130°C. While the powders and polymers were mixing, methyl poly ethylene glycol (MPEG) (MW 350, Acros Organics, Geel, Belgium) and heavy mineral oil (HMO) (Fisher Chemical, Pittsburgh, USA) were added to adjust the viscosity. The final compositions for each layer material are shown in Table I.

After formulating the compositions for each layer, the powder-loaded polymers were pressed into sheets (Model G50H, Wabash, Wabash, USA) at 150°C. The strong

ZrB_2 phase materials were pressed to a thickness of 0.46 ± .03 mm, while the weaker C-ZrB_2 phase was pressed to 0.18 ± .03 mm. After pressing, layers were stacked to provide a final part with approximately 23 weak phase layers and pressed at 150°C to produce laminate preforms. The preforms were cut to the size of a graphite hot press die using a razor blade and loaded into the die. Preforms then underwent binder burnout to remove the thermoplastic polymer and other organic processing aids. Burnout was accomplished using an atmosphere of 100 kPa of argon and a heating rate of 25°C per hour up to 125°C, then 5°C per hour up to 500°C where temperature was held for 2 hours to ensure complete burnout. After the isothermal hold the furnace power was shut off, allowing the specimen to cool to room temperature.

After burnout, the die containing the preform was transferred to a hot press (Model HP20-3060-20, Thermal technology, Santa Rosa, USA). The initial part of the heating cycle was conducted under a nominal vacuum of ~15 Pa. Preforms were heated at 50°C/min from room temperature to 1450°C. Temperature was held at 1450°C for one hour to allow the vacuum to recover to the nominal level. Heating was resumed at 50°C/min to 1650°C for another one hour isothermal hold for vacuum recovery. The purpose of the isothermal holds was to allow the sintering aids to react with and remove surface oxide impurities as described elsewhere.[25, 26, 27] After the second hold, the furnace was backfilled with argon to ~100 kPa. The furnace was heated at 30°C/min up to a maximum of 2050°C for densification where it was held for 1 hr. During the final ramp and hold, a uniaxial pressure of 32 MPa was applied. After the final hold, the furnace power was shut off and the system was allowed to cool. Once the temperature reached

1600°C the pressure was released, and the furnace was allowed to cool to room temperature.

Densified billets were removed from the die, surface ground to remove the outer layer, and cut into mechanical test bars using an automated surface grinder (Model FSG-3A818, Chevalier, Santa Fe Springs, USA). These mechanical test bars were 3 mm by 4 mm by 45 mm, which are size B-bars as defined in ASTM C1161. The bars were oriented such that the layers were parallel to the length of the bar (45 mm) and normal to the thickness (3 mm). Bars were polished on the tensile surface using successively finer diamond abrasives with a final abrasive size of 0.25 μm. The bars were then tested in 4-pt flexure at room temperature (Model 5881, Instron, Norwood, USA) and elevated temperatures (Model 33R4204, Instron, Norwood, USA) in accordance with ASTM C1161 (modified for elevated temperatures). In the flexure tests, the crosshead extension was controlled, and as the temperature increased the extension rate was increased in order to maintain linear elastic behavior as the load was applied. The extension rates used for flexure testing at the various temperatures are listed in Table II. Work of fracture was calculated by integrating the area under the load-displacement curve from the flexure test. Elastic work of fracture is the area under the curve during initial loading until the first load drop occurred. After the initial load drop, the area under the load-deflection curve was considered to be inelastic work of fracture.

The specimens were then mounted in an epoxy resin and cross sections were polished in steps down to 0.25 μm. The specimens were then removed from the epoxy and thermally etched at 1400°C using a heating rate of 50°C/min and a dwell time of 1 hour under a vacuum of ~15 Pa. Specimens were then coated with a mixture of gold and

palladium and images were taken using scanning electron microscopy (SEM; S4700, Hitachi, Tokyo, Japan) with an accelerating voltage of 5 kV. Energy dispersive spectroscopy (EDS) was also used to analyze sections of the microstructure. Average layer thicknesses and grain sizes were measured using ImageJ (National Institutes of Health, Bethesda, USA) using the average Feret's diameter over 500 grains.

3. RESULTS

The laminates consisted of alternating layers of predominantly uniform thickness (Figure 1). The area ratio of strong to weak phases in cross section was ~6.5:1, which means the volume ratio should be the same. Image analysis showed that the thickness of the average strong phase layer was 146 ± 23 μm and the thickness of the weak phase layers was 22 ± 8 μm. The specimens showed consistent layer thickness through most of the specimens, and it has been shown that specimens with parallel layers maximize crack deflection.[16] Parallel layers also reduce the frequency of discontinuities, which would allow two layers of the same composition to contact each other. Where discontinuities appear, it is possible for a crack to travel through just one material without the possibility of crack deflection, thereby reducing the advantage of the laminate architecture.

The microstructure of the strong layers is shown in Figure 2. The strong phase had an average ZrB_2 grain size of 18 ± 9 μm Dark inclusions were also present in the strong layers and EDS analysis of this material suggests that these were the remnants of the B_4C and C that were added as densification aids. These secondary phases were mainly located at grain boundary junctions and had an average diameter of approximately

6 ± 4 μm. The secondary phases extended along the grain boundaries, appearing as irregular shapes. Porosity also appeared in the structure, predominantly at the grain boundaries, although some intragranular pores were also observed.

The weak layers shown in Figure 3 appear to be the edges of aligned graphite platelets. Lighter spots within the weak layers had higher concentrations of Zr and B based on EDS. The Zr- and B-rich regions were regularly shaped, with an average size of 4.4 ± 1.7 μm. Presumably, these were ZrB_2 particles that had been added to the graphite. The grains of graphite were difficult to distinguish due to the plate-like texture of the particles and porosity that was present. Presumably, graphite in these specimens was not fully densified since graphite densification typically requires much higher temperatures.[28]

Figure 4 summarizes the strengths of the laminates as a function of temperature. At room temperature, the strength was 260 ± 36 MPa. This is approximately 70% of the strength of a conventional ZrB_2 ceramic processed by similar methods.[2] This ratio of strength between laminate and homogenous material is lower than would be predicted based on studies by Clegg et al.[11] The laminate materials studied by Clegg et al. showed similar strength to conventional ceramics. It is possible that the difference in strength for the current study is due to the presence of larger critical flaws introduced as a result of the specimen forming process used in this study. The size of the critical flaw in the current laminates was estimated using Griffith's criteria, which assumes that specimens exhibited brittle fracture. The equation that most accurately described this material was for surface flaws in a finite body (Eq 1).[29] For this equation K_I is the mode 1 fracture

toughness, σ is the flexure strength, F and Q account for the shape factor calculations for the geometry of the critical flaw, and a is the length of the critical flaw.

$$K_I = \sigma F \sqrt{\frac{\pi a}{Q}}$$

In this equation, each layer of the strong phase was treated as a separate body, meaning that the flaw size calculated was the size necessary to start a crack propagating in a single layer of material. Assuming a fracture toughness of 3.5 MPa√m for the strong phase layers in the laminates[3], it was determined that the critical flaw was about 30 μm. This corresponds to the maximum grain size observed in the strong phase. Observation of the fracture surfaces revealed that fractures originated at large grains on the tensile surfaces of the specimens, as seen in Figure 5. It is possible that by reducing the grain size in the specimen, by starting with smaller powder or going through more particle size reduction steps, would increase the strength of the laminates.

The laminate strengths were maximized at intermediate temperatures with strengths of 280 ± 54 MPa at 1400°C and 310 ± 10 MPa at 1600°C. As the temperature increased further, the strength decreased to 220 ± 9 MPa at 1800°C, and to 160 ± 14 MPa at 2000°C. The retention of strength by laminates from room temperature up to 1600°C indicates that the critical flaw in the material did not change as temperature increased. As temperatures approached 2000°C, it is likely that creep effects and grain boundary sliding limit the strength to levels below those seen at room temperature.[2] Overall, the laminates retained strength to high temperatures (~1800°C) because the critical flaw size did not change as a function of temperature.

The typical load-deflection curves for the laminates are shown in Figure 6, while the corresponding cross-sectional images are shown in Figure 7. As temperature increased, the amount of crack deflection tended to decrease, reaching a minimum at 2000°C. This trend could be due to the increased loading rate used at higher temperatures. The loading rate was used to maintain linear-elastic behavior as temperature increased.[2, 16] Cracks that formed also tended to travel through the center of the weak layers, as opposed to along the interface between strong and weak layers, as seen in Figure 8.

The inelastic work of fracture increased from room temperature to 1600°C, and then decreased above 1600°C as the testing temperature approached 2000°C. In addition, the ratio of inelastic work of fracture to total work of fracture decreased as temperature increased. At room temperature, the inelastic work of fracture was 0.7 kJ/m^2 (38% of the total work of fracture), while at 1600°C the inelastic work of fracture was 2.5 kJ/m^2 (31%) and at 2000°C it was 0.07 kJ/m^2 (5%) (Table III). The large standard deviation, as seen in Figure 9 was due to the variability in crack deflection, which was most likely due to inconsistencies in the layer thicknesses of the laminates. The levels of inelastic work of fracture shown by these specimens show that the laminate structure is more resistant to catastrophic brittle failure than conventional ZrB_2 ceramics.

4. CONCLUSIONS

Zirconium diboride-based laminates were produced using alternating layers of strong ZrB_2 ceramics and weak layers of graphite containing 10 vol% ZrB_2. Laminates were densified by hot pressing at 2050°C under 32 MPa. The laminates exhibited layers

that were parallel and evenly spaced, with strong layers being on average 4 times thicker than the weak layers. The microstructure of the strong layers showed evidence of B_4C and C inclusions. The laminates had a strength of ~250 MPa at room temperature, retaining this strength up to 1800°C. The strength of these laminates was limited by the grain size of the strong phase, and the critical flaw size remains constant until the temperature rises above 1800°C. The inelastic work of fracture at room temperature was ~0.65 kJ/m^2 at room temp with a maximum of ~2.5 kJ/m^2 at 1600°C. The large deviation in the values was likely due to variations in crack paths for different specimens. Crack deflection occurred near the center of the weak layers rather than the interfaces between layers. The laminates produced maintained flexure strengths in excess of 200 MPa up to 1800°C while successfully increasing the work of fracture at all temperatures tested.

ACKNOWLEDGMENTS

The authors would like to acknowledge financial support from the Aerospace Materials For Extreme Environments program (program manager Ali Sayir) in the US Air Force Office of Scientific Research through grant FA9550-14-1-0385. The authors would also like to thank the Advanced Materials Characterization Laboratory at Missouri University of Science and Technology for the use of their characterization equipment.

REFERENCES

1. N. L. Okamoto, M. Kusakari, K. Tanaka, H. Inui, and S. Otani, "Anisotropic elastic constants and thermal expansivities in monocrystal CrB2, TiB2, and ZrB2," Acta Materialia, 58[1] 76-84 (2010).
2. E. W. Neuman, G. E. Hilmas, and W. G. Fahrenholtz, "Strength of Zirconium Diboride to 2300°C," Journal of the American Ceramic Society, 96[1] 47-50 (2013).
3. A. L. Chamberlain, W. G. Fahrenholtz, and G. E. Hilmas, "Pressureless Sintering of Zirconium Diboride," Journal of the American Ceramic Society, 89[2] 450-56 (2006).
4. S.-Q. Guo, J.-M. Yang, H. Tanaka, and Y. Kagawa, "Effect of thermal exposure on strength of ZrB2-based composites with nano-sized SiC particles," Composites Science and Technology, 68[14] 3033-40 (2008).
5. E. W. Neuman, G. E. Hilmas, and W. G. Fahrenholtz, "Processing, microstructure, and mechanical properties of large-grained zirconium diboride ceramics," Materials Science and Engineering: A, 670 196-204 (2016).
6. L. Xu, C. Huang, H. Liu, B. Zou, H. Zhu, G. Zhao, and J. Wang, "Study on in-situ synthesis of ZrB2 whiskers in ZrB2–ZrC matrix powder for ceramic cutting tools," International Journal of Refractory Metals and Hard Materials, 37 98-105 (2013).
7. M. Okabe, H. Mori, K. Kuwabara, S. Ogata, Y. Shia, and K. Sakai, "Continuous measurement of molten steel temperature," Nippon Steel Technical Report[49] 23-28 (1991).
8. A. Cecere, R. Savino, C. Allouis, and F. Monteverde, "Heat transfer in ultra-high temperature advanced ceramics under high enthalpy arc-jet conditions," International Journal of Heat and Mass Transfer, 91 747-55 (2015).

9. E. W. Neuman, G. E. Hilmas, and W. G. Fahrenholtz, "A high strength alumina-silicon carbide-boron carbide triplex ceramic," Ceramics International, 43[10] 7958-62 (2017).
10. K. C. Goretta, T. A. Cruse, D. Singh, J. L. Routbort, A. R. de Arellano-Lopez, T. S. Orlova, and B. I. Smirnov, "Ceramic fibrous monolithic structures," Composite Structures, 66[1–4] 547-53 (2004).
11. W. J. Clegg, "The fabrication and failure of laminar ceramic composites," Acta Metallurgica et Materialia, 40[11] 3085-93 (1992).
12. M. Oechsner, C. Hillman, and F. F. Lange, "Crack Bifurcation in Laminar Ceramic Composites," Journal of the American Ceramic Society, 79[7] 1834-38 (1996).
13. K. Kendall, "Transition between Cohesive and Interfacial Failure in a Laminate," Proceedings of the Royal Society of London. Series A, Mathematical and Physical Sciences, 344 287-302 (1975).
14. W. J. Clegg, "Controlling Cracks in Ceramics," Science, 286[5442] 1097-99 (1999).
15. J. B. Davis, A. Kristoffersson, E. Carlström, and W. J. Clegg, "Fabrication and Crack Deflection in Ceramic Laminates with Porous Interlayers," Journal of the American Ceramic Society, 83[10] 2369-74 (2000).
16. M.-Y. He and J. W. Hutchinson, "Crack Deflection at an Interface between Dissimilar Elastic Materials," International Journal of Solids and Structures, 25[9] 1053-67 (1989).
17. W. J. Clegg, S. J. Howard, W. Lee, A. J. Phillipps, and R. A. Stewart, "Interfacial cracking in ceramic laminates," Composite Interfaces, 2[5] 337-49 (1994).
18. "Standard Test Method for Flexural Strength of Advanced Ceramics at Ambient Temperature." in. ASTM International, 2013.

19. S. Baskaran and J. W. Halloran, "Fibrous Monolithic Ceramics: II, Flexural Strength and Fracture Behavior of the Silicon Carbide/Graphite System," Journal of the American Ceramic Society, 76[9] 2217-24 (1993).

20. W. J. Clegg, K. Kendall, N. M. Alford, T. W. Button, and J. D. Birchall, "A Simple Way to Make Tough Ceramics," Nature, 347[6292] 455 (1990).

21. H. Chan, "LAYERED CERAMICS: Processing and Mechanical Behavior," Annual Review of Materials Science, 27[1] 249-82 (1997).

22. D. J. Green, P. Z. Cai, and G. L. Messing, "Residual Stresses in Alumina-Zirconia Laminates," Journal of the European Ceramic Society, 19 2511-17 (1999).

23. C. Hillman, Z. Suo, and F. F. Lange, "Cracking of Laminates Subjected to Biaxial Tensile Stresses," Journal of the American Ceramic Society, 79[8] 2127-33 (1996).

24. D. Kovar, B. H. King, R. W. Trice, and J. W. Halloran, "Fibrous Monolithic Ceramics," *Journal of the American Ceramic Society*, 80[10] 2471-87 (1997).

25. W. G. Fahrenholtz, G. E. Hilmas, S. C. Zhang, and S. Zhu, "Pressureless Sintering of Zirconium Diboride: Particle Size and Additive Effects," Journal of the American Ceramic Society, 91[5] 1398-404 (2008).

26. S. Zhu, W. G. Fahrenholtz, G. E. Hilmas, and S. C. Zhang, "Pressureless Sintering of Zirconium Diboride Using Boron Carbide and Carbon Additions," Journal of the American Ceramic Society, 90[11] 3660-63 (2007).

27. S. C. Zhang, G. E. Hilmas, and W. G. Fahrenholtz, "Pressureless Densification of Zirconium Diboride with Boron Carbide Additions," Journal of the American Ceramic Society, 89[5] 1544-50 (2006).

28. R. K. Carlson and J. J. Ferritto, "Manufacture of high density, high strength isotropic graphite." in. Google Patents, 1980.

29. T. L. Anderson and T. Anderson, "Fracture Mechanics: Fundamentals and Applications." CRC Press, (2005).

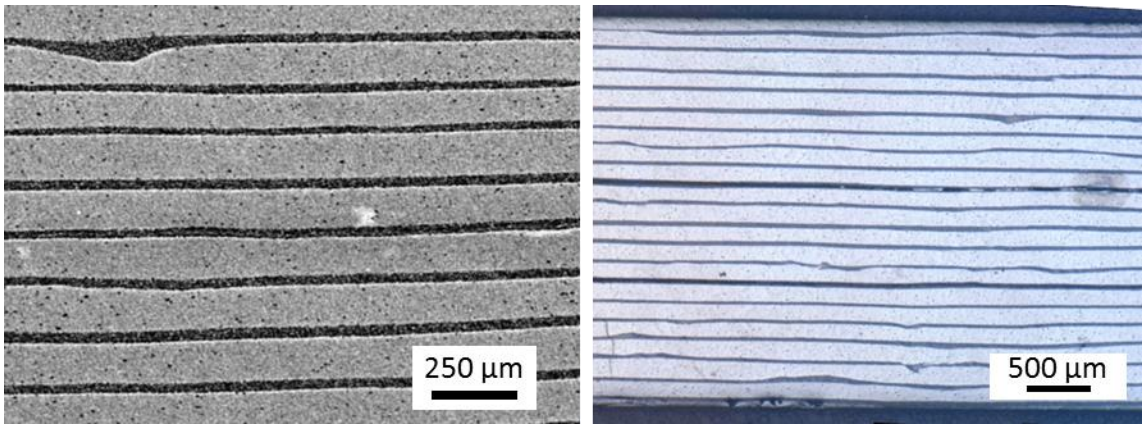

Figure 1. Mesostructure of a ZrB_2/C-10 vol% ZrB_2 laminate composite.

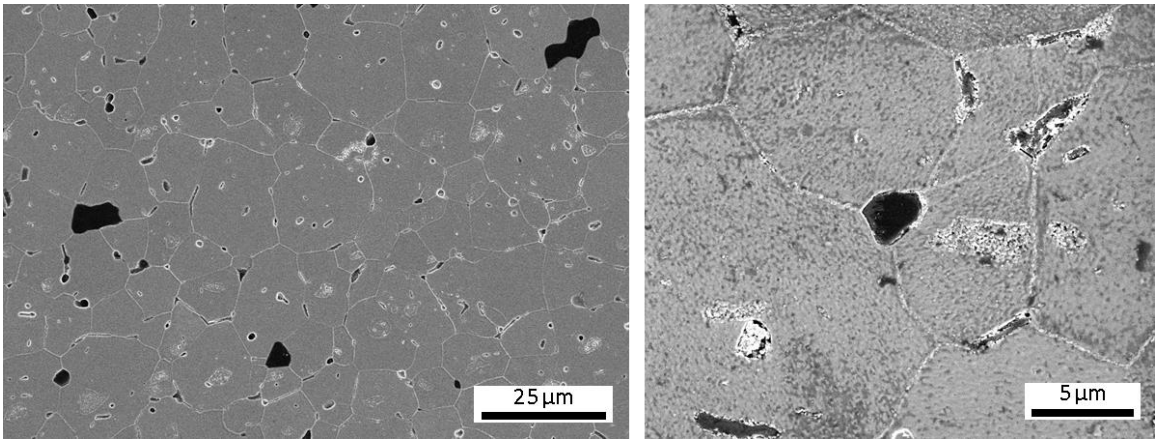

Figure 2. Microstructure of the strong layer showing ZrB_2 grains, second phases, and porosity.

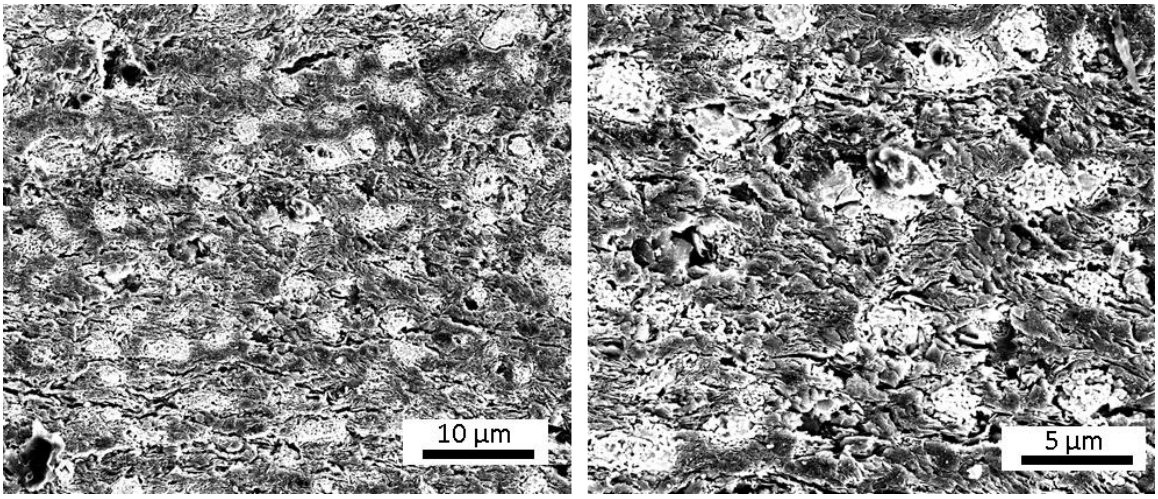

Figure 3. Microstructure of the weak layer. Brighter regions are clusters of ZrB_2 in the graphite matrix.

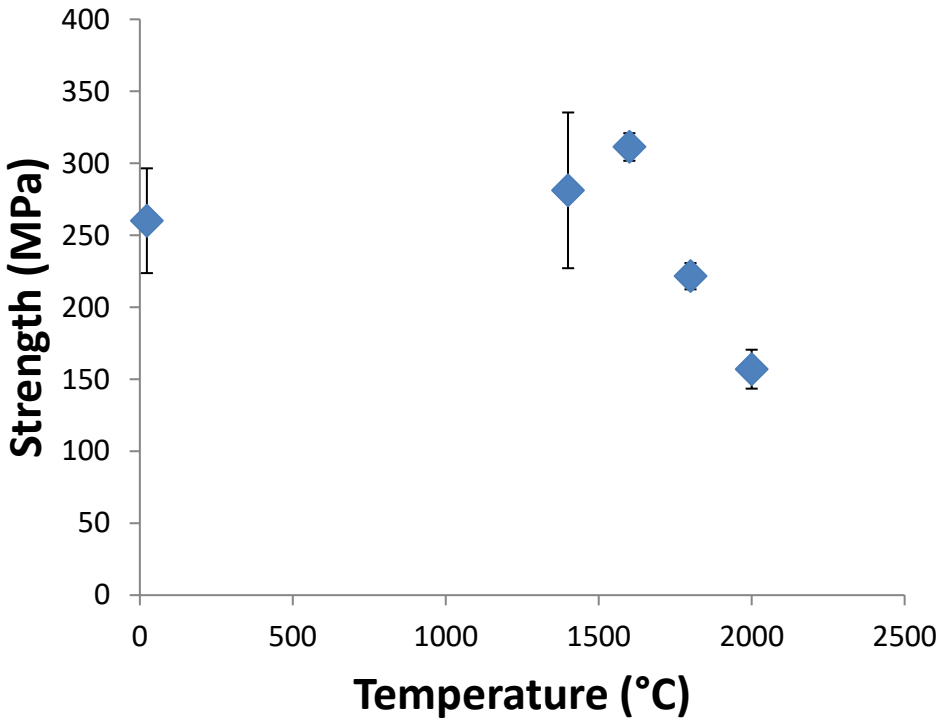

Figure 4. Flexure strength as a function of temperature for ZrB_2/C-10vol% ZrB_2 laminates.

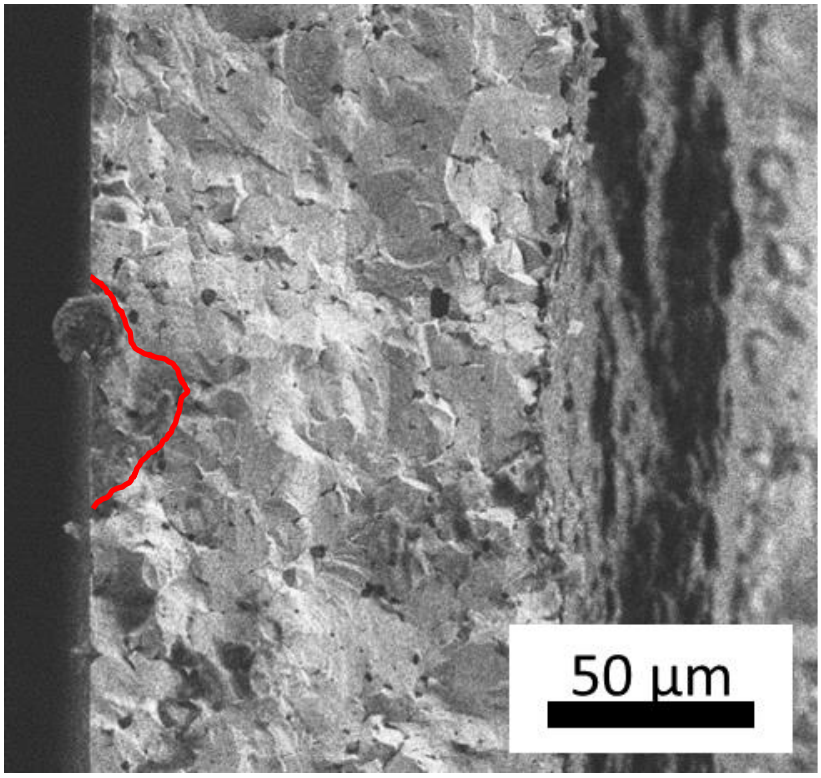

Figure 5. Fracture surface of a laminate specimen fractured at room temperature.

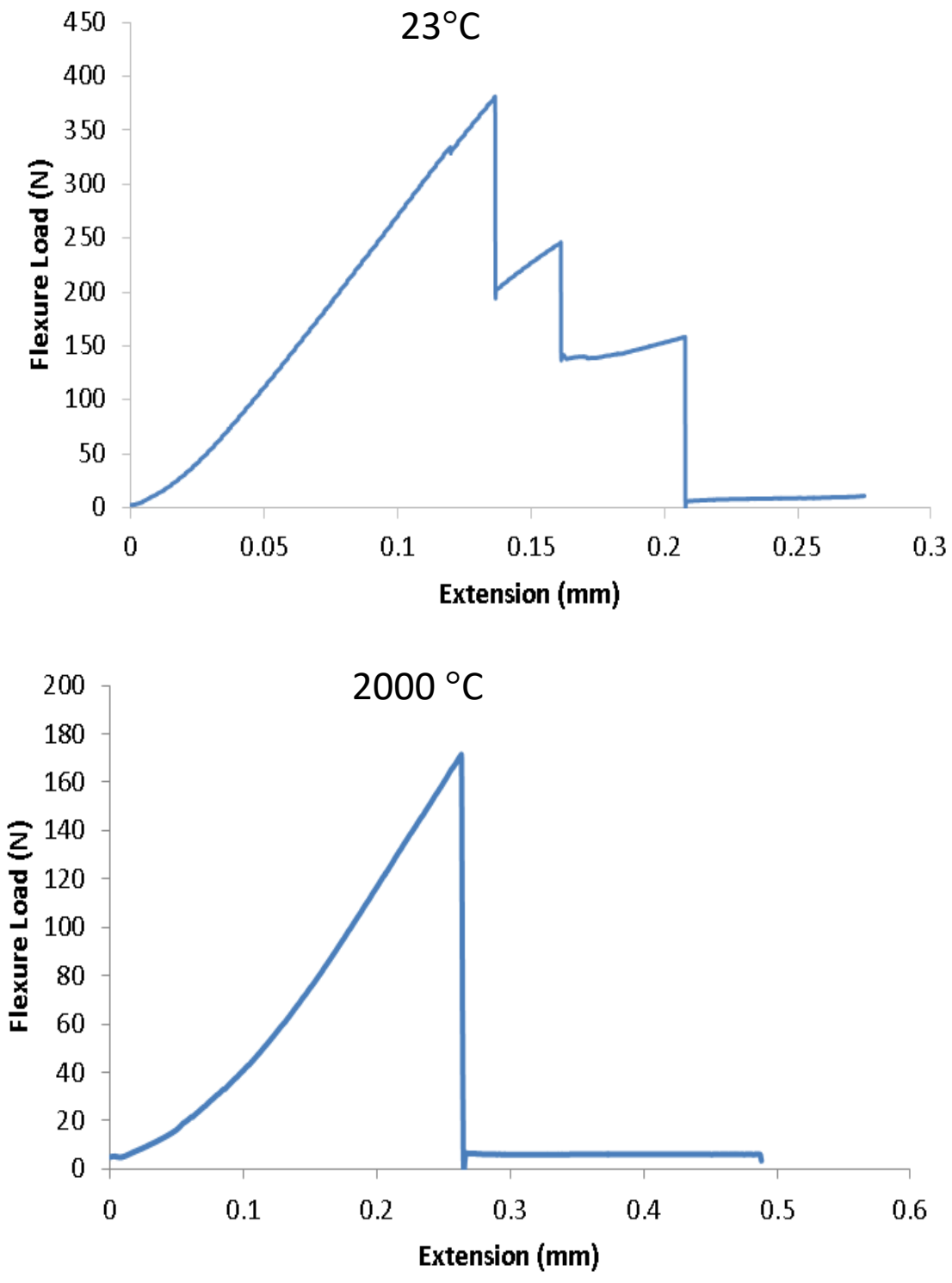

Figure 6. Flexure load vs extension for bars at room temperature (top) and 2000°C (bottom).

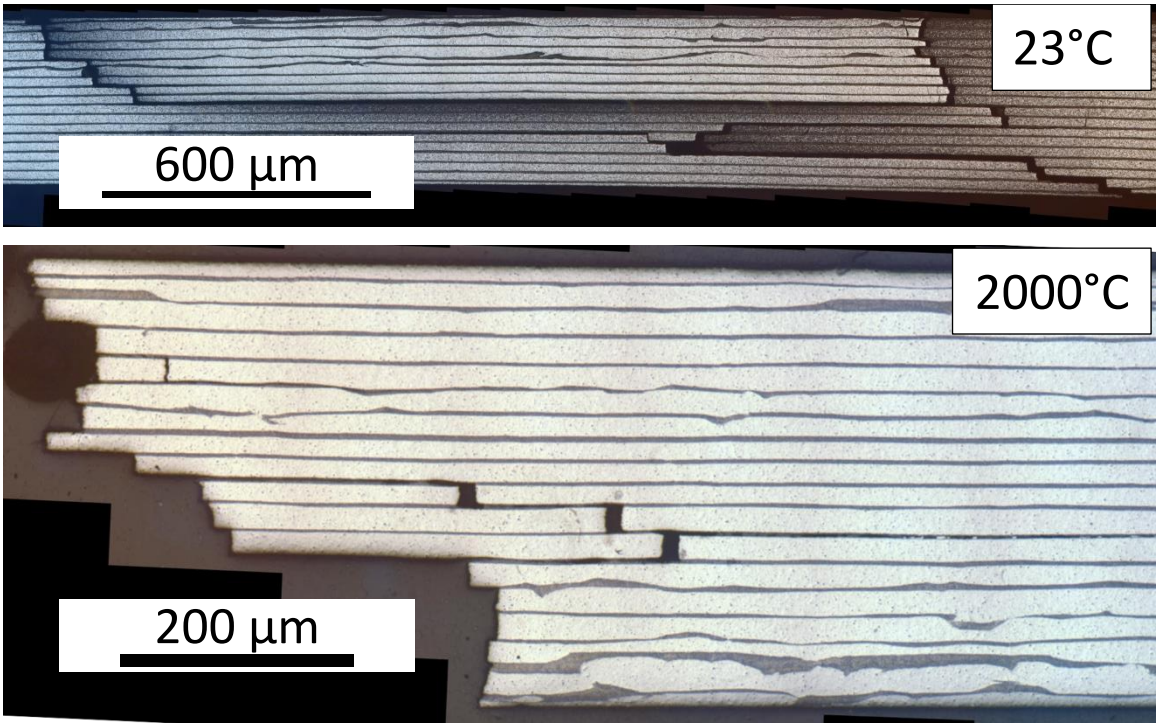

Figure 7. Cross section of bars tested at room temperature (top) and 2000°C (bottom). The bottom of each image is the tensile surface of the specimen.

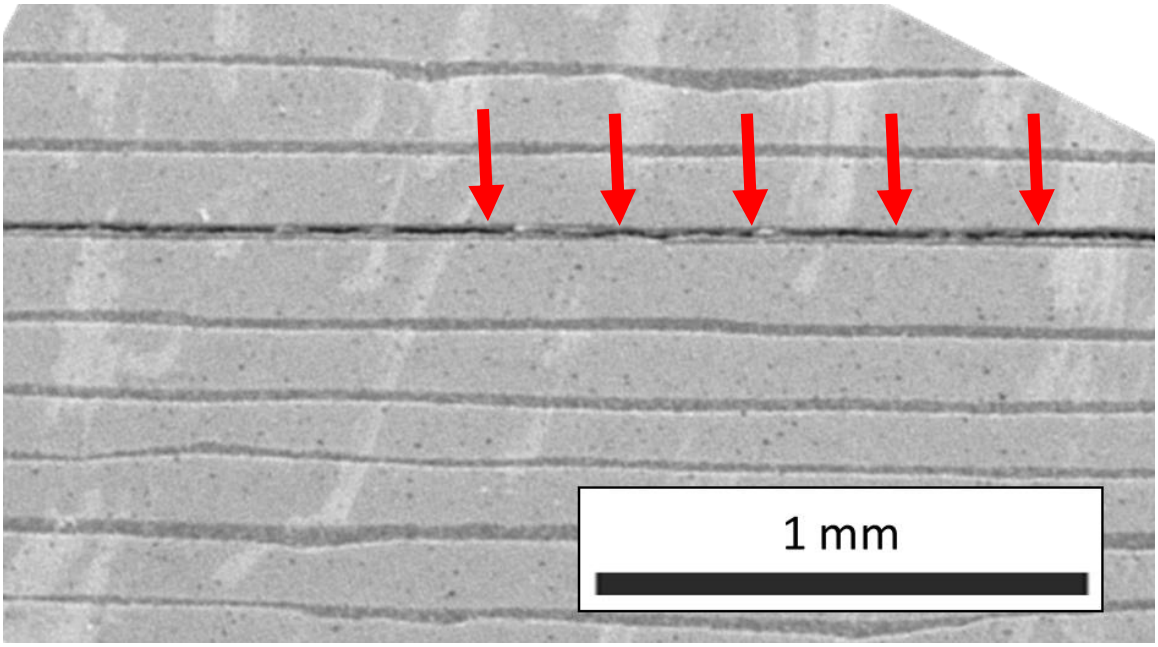

Figure 8. Cross section of bar tested at 1400°C showing crack path through the graphite layer. Arrows point to the crack travelling through the center of the weak phase.

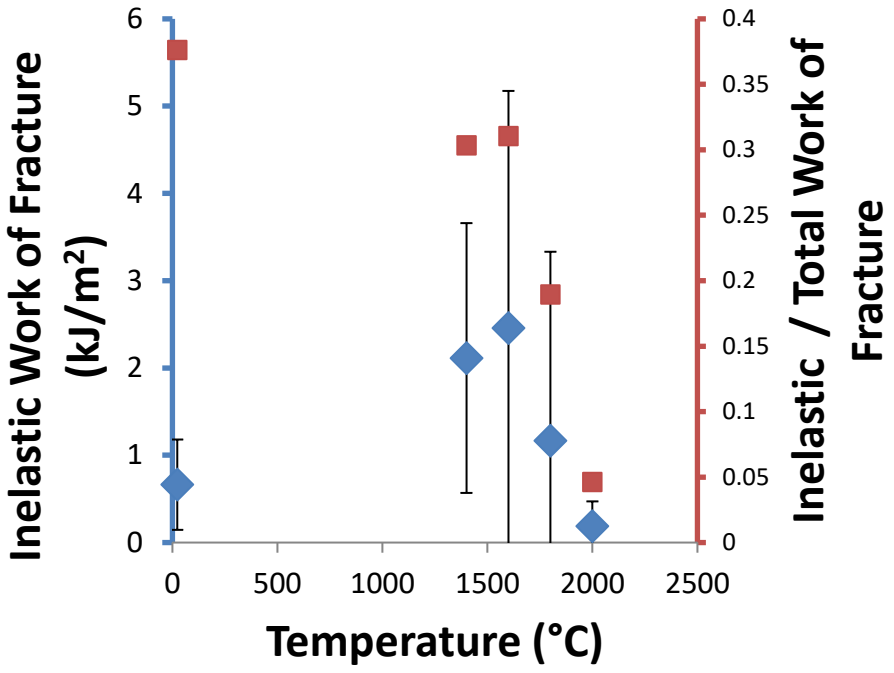

Figure 9. Inelastic work of fracture and fraction of work of fracture that was inelastic as a function of temperature. Diamonds correspond to the measured inelastic work of fracture, and the squares correspond to the ratio of the inelastic work of fracture to total work of fracture.

Table 1. Compositions of strong and weak layers for ZrB_2-based laminates.

	Volume Fraction	
Material	Strong Phase	Weak Phase
ZrB_2	0.524	0.037
Graphite	-	0.336
B_4C	0.015	-
Carbon Black	0.020	-
EEA	0.354	0.579
HMO	0.080	0.039
MPEG	0.008	0.008
Total	1.001	0.999

Table 2. Crosshead displacement loading rates and strain rates for flexure testing at elevated temperatures.

Temperature (°C)	Crosshead displacement (mm/min)	Strain Rate
23	0.1	0.00125
1400	0.2	0.0025
1600	0.4	0.005
1800	0.6	0.007
2000	1.5	0.017

Table 3. Mechanical properties of ZrB_2-based laminate specimens.

Temperature	Strength	Inelastic Work of Fracture	Ratio of Inelastic to Total Work of Fracture
°C	MPa	kJ/m^2	
23	260 ± 36	0.6 ± 0.5	0.38
1400	314 ± 54	2.1 ± 1.6	0.30
1600	311 ± 10	2.5 ± 2.7	0.31
1800	225 ± 10	1.2 ± 2.2	0.19
2000	144 ± 14	0.19 ± 0.28	0.05

3. CONCLUSIONS

This research focused on the fabrication and properties of transition metal diboride based ceramics with engineered architectures. Foam and laminate structures were made from TiB_2 and ZrB_2 respectively, and then tested to determine their properties. Testing for each specimen was performed to find the answers to the questions raised in the introduction.

Can a TiB_2 foam that retains a high intrinsic hardness be produced? What strength values would this structure exhibit?

The first paper focused on the fabrication of a TiB_2 foam, and showed that it is possible to produce TiB_2 foams. Testing the hardness of the foam specimens also revealed that the material behaved similarly to dense TiB_2, with hardness values around 17 GPa. This is comparable to other studies for TiB_2 ceramics in which the measured hardness value for these specimens was lower than the intrinsic hardness due to microcracking. Microcracking was likely to be present in this specimen, because the grain size was large enough that anisotropic thermal stresses between grains induce fractures in the microstructure.

Will a laminate of ZrB_2/ C–10 vol% ZrB_2 deflect cracks at room and high temperatures? What is the work of fracture for specimens that do deflect cracks?

In the second paper, a laminate was produced composed of ZrB_2 and C. Testing was performed at temperatures ranging from room temperature to 2000°C, and laminates showed a larger degree of crack deflection at lower temperatures than higher temperatures, as evidenced by the work of fracture measured at each temperature. The

ratio of the inelastic work of fracture to the total work of fracture decreased as the temperature increased.

How do the ZrB_2/ C–10 vol% ZrB_2 laminates fail, and do they exhibit similar strength to homogenous ZrB_2 at all temperatures?

Laminate specimens were tested in 4-pt flexure to determine their strength at different temperatures. The strength of the laminates was maintained from room temperature up to 1600°C, at around 260 MPa. Strength decreased when tested at temperatures 1800°C and above. The decrease in strength is similar to the behavior seen in high temperature tests of homogenous ZrB_2 specimens. After analyzing fracture surfaces, it was determined that the critical flaw was the grain size of the strong phase material. The laminate specimens exhibited a maximum grain size of around 30 μm, which is consistent with the strength predicted using Griffith flaw size equations under the assumption that the critical flaw is along the edge of the specimen.

4. FUTURE WORK

The focus of this research was on producing a structurally stable foam and a laminate material using diboride ceramics.

For the TiB_2 foams, it is important to control the grain size and relative density. Beyond influencing the strength of the specimens, a large grain size causes significant microcracking in TiB_2. This effect has been seen in materials with a grain size as small as approximately 5 μm. Reducing the grain size below this threshold should increase the strength and the hardness of the foams, potentially increasing its usefulness. Performing a study on the properties of a foam with a small grain size should give a better idea of the performance of this material.

Another important factor controlling the mechanical properties of foam materials is the average thickness of the struts. As the strut size increases, the strength and modulus of the foam are increased along with the bulk density. A series of experiments evaluating the strength and porosity of the foam structures as a function of strut thickness would show the tradeoff between the density and strength of the foam. This information would be useful in determining the different strut thickness necessary for foams to be used in various applications.

For foam materials, another factor that can be controlled is the amount of material within the struts. This is primarily an issue for materials produced using the replication technique, where burnout of the polymer structure leaves additional porosity inside the struts of the foam. It may be possible to infiltrate the struts with additional slurry after burnout, raising the overall density but leaving the amount of open porosity unaffected.

For the ZrB_2 laminates, reducing the grain size will result in an increased strength across all temperatures. In the tested specimens, the strength limiting feature was the large grain size and so a reduction in the grain size will result in an increase in strength. The grain size may be decreased through further milling the powder or through the addition of additional secondary phases.

The mechanical properties of laminates may also vary with different relative layer thicknesses. It is possible that decreasing the thicknesses of both layers and keeping the same volume ratio of the strong and weak phases, would result in a greater amount of crack deflection due to the increased number of interfaces. To test this hypothesis, a series of experiments focused on flexure testing laminates with different layer thicknesses can be tested, though care must be taken to avoid discontinuities occurring when the layer thicknesses decrease.

REFERENCES

1. W. G. Fahrenholtz, G. E. Hilmas, I. G. Talmy, and J. A. Zaykoski, "Refractory Diborides of Zirconium and Hafnium," Journal of the American Ceramic Society, 90[5] 1347-64 (2007).
2. B. Basu, G. B. Raju, and A. K. Suri, "Processing and properties of monolithic TiB2 based materials," International Materials Reviews, 51[6] 352-74 (2006).
3. A. K. Mallik, N. C. Acikbas, F. Kara, H. Mandal, and D. Basu, "A comparative study of SiAlON ceramics," Ceramics International, 38[7] 5757-67 (2012).
4. H. Itoh, S. Naka, T. Matsudaira, and H. Hamamoto, "Preparation of Titanium Diboride sintered compacts by hot pressing," J Mater Sci, 25[1] 533-36 (1990).
5. F. W. Vahldiek and S. A. Mersol, "Slip and microhardness of IVa to via refractory materials," Journal of the Less Common Metals, 55[2] 265-78 (1977).
6. W. Wang, Z. Fu, H. Wang, and R. Yuan, "Influence of hot pressing sintering temperature and time on microstructure and mechanical properties of TiB2 ceramics," Journal of the European Ceramic Society, 22[7] 1045-49 (2002).
7. J. L. Murray, P. K. Liao, and K. E. Spear, "The B-Ti (Boron-Titanium) system," Bulletin of Alloy Phase Diagrams, 7[6] 550-55 (1986).
8. M. F. Ashby and R. F. M. Medalist, "The mechanical properties of cellular solids " Metallurgical Transactions A, 14[9] 1755-69 (1983).
9. M. V. Twigg and J. T. Richardson, "Fundamentals and Applications of Structured Ceramic Foam Catalysts," Industrial & Engineering Chemistry Research, 46[12] 4166-77 (2007).

10. M. Syvertsen and S. Bao, "Performance Evaluation of Two Different Industrial Foam Filters with LiMCA II Data," Metall and Materi Trans B [1-8] (2014).

11. Z. Wu, L. Sun, Z. Tian, J. Wang, J. Li, and Z. Hu, "Preparation and properties of reticulated porous γ-Y2Si2O7 ceramics with high porosity and relatively high strength," Ceramics International, 40[7, Part A] 10013-20 (2014).

12. A. Cecere, R. Savino, C. Allouis, and F. Monteverde, "Heat transfer in ultra-high temperature advanced ceramics under high enthalpy arc-jet conditions," International Journal of Heat and Mass Transfer, 91 747-55 (2015).

13. A. L. Chamberlain, W. G. Fahrenholtz, G. E. Hilmas, and D. T. Ellerby, "High-Strength Zirconium Diboride-Based Ceramics," Journal of the American Ceramic Society, 87[6] 1170-72 (2004).

14. T. A. Parthasarathy, R. A. Rapp, M. Opeka, and R. J. Kerans, "A model for the oxidation of ZrB2, HfB2 and TiB2," Acta Materialia, 55[17] 5999-6010 (2007).

15. H. Chan, "LAYERED CERAMICS: Processing and Mechanical Behavior," Annual Review of Materials Science, 27[1] 249-82 (1997).

16. J. B. Davis, A. Kristoffersson, E. Carlström, and W. J. Clegg, "Fabrication and Crack Deflection in Ceramic Laminates with Porous Interlayers," Journal of the American Ceramic Society, 83[10] 2369-74 (2000).

17. D. J. Green, P. Z. Cai, and G. L. Messing, "Residual Stresses in Alumina-Zirconia Laminates," Journal of the European Ceramic Society, 19 2511-17 (1999).

18. W. J. Clegg, S. J. Howard, W. Lee, A. J. Phillipps, and R. A. Stewart, "Interfacial cracking in ceramic laminates," Composite Interfaces, 2[5] 337-49 (1994).

19. M.-Y. He and J. W. Hutchinson, "Crack Deflection at an Interface between Dissimilar Elastic Materials," International Journal of Solids and Structures, 25[9] 1053-67 (1989).

20. N. L. Okamoto, M. Kusakari, K. Tanaka, H. Inui, and S. Otani, "Anisotropic elastic constants and thermal expansivities in monocrystal CrB2, TiB2, and ZrB2," Acta Materialia, 58[1] 76-84 (2010).

21. J. W. Lawson, C. W. Bauschlicher, and M. S. Daw, "Ab Initio Computations of Electronic, Mechanical, and Thermal Properties of ZrB2 and HfB2," Journal of the American Ceramic Society, 94[10] 3494-99 (2011).

22. Y.-H. Koh, S.-Y. Lee, and H.-E. Kim, "Oxidation Behavior of Titanium Boride at Elevated Temperatures," Journal of the American Ceramic Society, 84[1] 239-41 (2001).

23. A. Kulpa and T. Troczynski, "Oxidation of TiB2 Powders below 900°C," Journal of the American Ceramic Society, 79[2] 518-20 (1996).

24. S. Baik and P. F. Becher, "Effect of Oxygen Contamination on Densification of TiB2 " Journal of the American Ceramic Society, 70[8] 527-30 (1987).

25. M.-A. Einarsrud, E. Hagen, G. Pettersen, and T. Grande, "Pressureless Sintering of Titanium Diboride with Nickel, Nickel Boride, and Iron Additives," Journal of the American Ceramic Society, 80[12] 3013-20 (1997).

26. J.-H. Park, Y.-H. Lee, Y.-H. Koh, H.-E. Kim, and S. Su Baek, "Effect of Hot-Pressing Temperature on Densification and Mechanical Properties of Titanium Diboride with Silicon Nitride as a Sintering Aid," Journal of the American Ceramic Society, 83[6] 1542-44 (2000).

27. M. K. Ferber, P. F. Becher, and C. B. Finch, "Effect of Microstructure on the Properties of TiB2 Ceramics," Journal of the American Ceramic Society, 66[1] C-2-C-3 (1983).

28. E. Kang and C. Kim, "Improvements in mechanical properties of TiB2 by the dispersion of B4C particles," J Mater Sci, 25[1] 580-84 (1990).

29. J.-H. Park, Y.-H. Koh, H.-E. Kim, C. S. Hwang, and E. S. Kang, "Densification and Mechanical Properties of Titanium Diboride with Silicon Nitride as a Sintering Aid," Journal of the American Ceramic Society, 82[11] 3037-42 (1999).

30. S.-Q. Guo, J.-M. Yang, H. Tanaka, and Y. Kagawa, "Effect of thermal exposure on strength of ZrB2-based composites with nano-sized SiC particles," Composites Science and Technology, 68[14] 3033-40 (2008).

31. E. W. Neuman, G. E. Hilmas, and W. G. Fahrenholtz, "Strength of Zirconium Diboride to 2300°C," Journal of the American Ceramic Society, 96[1] 47-50 (2013).

32. F. Monteverde and A. Bellosi, "Effect of the addition of silicon nitride on sintering behaviour and microstructure of zirconium diboride," Scripta Materialia, 46[3] 223-28 (2002).

33. S. C. Zhang, G. E. Hilmas, and W. G. Fahrenholtz, "Pressureless Densification of Zirconium Diboride with Boron Carbide Additions," Journal of the American Ceramic Society, 89[5] 1544-50 (2006).

34. S. Zhu, W. G. Fahrenholtz, G. E. Hilmas, and S. C. Zhang, "Pressureless Sintering of Zirconium Diboride Using Boron Carbide and Carbon Additions," Journal of the American Ceramic Society, 90[11] 3660-63 (2007).

35. S. Zhu, W. G. Fahrenholtz, G. E. Hilmas, and S. C. Zhang, "Pressureless sintering of carbon-coated zirconium diboride powders," Materials Science and Engineering: A, 459[1–2] 167-71 (2007).

36. L. Xu, C. Huang, H. Liu, B. Zou, H. Zhu, G. Zhao, and J. Wang, "Study on in-situ synthesis of ZrB2 whiskers in ZrB2–ZrC matrix powder for ceramic cutting tools," International Journal of Refractory Metals and Hard Materials, 37 98-105 (2013).

37. M. Okabe, H. Mori, K. Kuwabara, S. Ogata, Y. Shia, and K. Sakai, "Continuous measurement of molten steel temperature," Nippon Steel Technical Report[49] 23-28 (1991).

38. A. L. Chamberlain, W. G. Fahrenholtz, and G. E. Hilmas, "Pressureless Sintering of Zirconium Diboride," Journal of the American Ceramic Society, 89[2] 450-56 (2006).

39. E. W. Neuman, G. E. Hilmas, and W. G. Fahrenholtz, "Processing, microstructure, and mechanical properties of large-grained zirconium diboride ceramics," Materials Science and Engineering: A, 670 196-204 (2016).

40. M. S. Asl, M. G. Kakroudi, and S. Noori, "Hardness and toughness of hot pressed ZrB2–SiC composites consolidated under relatively low pressure," Journal of Alloys and Compounds, 619[0] 481-87 (2015).

41. J. Watts, G. Hilmas, W. G. Fahrenholtz, D. Brown, and B. Clausen, "Measurement of thermal residual stresses in ZrB2–SiC composites," Journal of the European Ceramic Society, 31[9] 1811-20 (2011).

42. J. Banhart, "Manufacture, characterisation and application of cellular metals and metal foams," Progress in Materials Science, 46[6] 559-632 (2001).

43. D. A. Heirschfeld, "Processing of Porous Oxide Ceramics," Key Engineering Materials 115 65-80 (1995).

44. L. Montanaro, "Ceramic foams by powder processing," Journal of the European Ceramic Society, 18[9] 1339-50 (1998).

45. C. Vakifahmetoglu, D. Zeydanli, and P. Colombo, "Porous polymer derived ceramics," Materials Science and Engineering: R: Reports, 106 1-30 (2016).

46. M. Emmel, C. G. Aneziris, F. Sponza, S. Dudczig, and P. Colombo, "In situ spinel formation in Al2O3–MgO–C filter materials for steel melt filtration," Ceramics International, 40[8, Part B] 13507-13 (2014).

47. H. I. Bakan and K. Korkmaz, "Synthesis and properties of metal matrix composite foams based on austenitic stainless steels –titanium carbonitrides," Materials & Design, 83 154-58 (2015).

48. F. C. Buciuman and B. Kraushaar-Czarnetzki, "Ceramic Foam Monoliths as Catalyst Carriers. 1. Adjustment and Description of the Morphology," Industrial & Engineering Chemistry Research, 42[9] 1863-69 (2003).

49. C. Voigt, "The influence of the measurement parameters on the crushing strength of reticulated ceramic foams," Journal of Materials Research, 28[17] 2288-99 (2013).

50. C. Voigt, T. Zienert, P. Schubert, C. G. Aneziris, and J. Hubálková, "Reticulated Porous Foam Ceramics with Different Surface Chemistries," Journal of the American Ceramic Society, 97[7] 2046-53 (2014).

51. Q. Z. Chen, A. R. Boccaccini, H. B. Zhang, D. Z. Wang, and M. J. Edirisinghe, "Improved Mechanical Reliability of Bone Tissue Engineering (Zirconia) Scaffolds by Electrospraying," Journal of the American Ceramic Society, 89[5] 1534-39 (2006).

52. A. S. Apkar'yan, "Investigation of the Density of Granular Foam-Glass Ceramic by Mathematical Modeling," Glass Ceram, 71[5-6] 194-97 (2014).

53. J. R. Jones, L. M. Ehrenfried, and L. L. Hench, "Optimising bioactive glass scaffolds for bone tissue engineering," Biomaterials, 27[7] 964-73 (2006).

54. P. A. I. Sepulveda and J. G. P. Binner, "Processing of cellular ceramics by foaming and in situ polymerisation of organic monomers," Journal of the European Ceramic Society, 19[12] 2059-66 (1999).

55. L. P. Lefebvre, J. Banhart, and D. C. Dunand, "Porous Metals and Metallic Foams: Current Status and Recent Developments," Advanced Engineering Materials, 10[9] 775-87 (2008).

56. S. K. Goel and E. J. Beckman, "Generation of microcellular polymeric foams using supercritical carbon dioxide. I: Effect of pressure and temperature on nucleation," Polymer Engineering and Science, 34[14] 1137-48 (1994).

57. J. T. Muth, P. G. Dixon, L. Woish, L. J. Gibson, and J. A. Lewis, "Architected cellular ceramics with tailored stiffness via direct foam writing," Proceedings of the National Academy of Sciences, 114[8] 1832-37 (2017).

58. D. A. Snelling, C. B. Williams, C. T. A. Suchicital, and A. P. Druschitz, "Binder jetting advanced ceramics for metal-ceramic composite structures," The International Journal of Advanced Manufacturing Technology 1-15 (2017).

59. Q. Fu, E. Saiz, M. N. Rahaman, and A. P. Tomsia, "Toward Strong and Tough Glass and Ceramic Scaffolds for Bone Repair," Advanced Functional Materials, 23[44] 5461-76 (2013).

60. S. Sihn and A. K. Roy, "Modeling and prediction of bulk properties of open-cell carbon foam," Journal of the Mechanics and Physics of Solids, 52[1] 167-91 (2004).

61. S. K. Maiti, L. J. Gibson, and M. F. Ashby, "Deformation and energy absorption diagrams for cellular solids," Acta Metallurgica, 32[11] 1963-75 (1984).

62. E. Rezaei, G. Bianchi, S. Gianella, and A. Ortona, "On the nonlinear mechanical behavior of macroporous cellular ceramics under bending," Journal of the European Ceramic Society, 34[10] 2133-41 (2014).

63. L. F. Nielsen, "Elasticity and Damping of Porous Materials and Impregnated Materials," Journal of the American Ceramic Society, 67[2] 93-98 (1984).

64. S. Baskaran and J. W. Halloran, "Fibrous Monolithic Ceramics: II, Flexural Strength and Fracture Behavior of the Silicon Carbide/Graphite System," Journal of the American Ceramic Society, 76[9] 2217-24 (1993).

65. W. J. Clegg, "The fabrication and failure of laminar ceramic composites," Acta Metallurgica et Materialia, 40[11] 3085-93 (1992).

66. W. J. Clegg, K. Kendall, N. M. Alford, T. W. Button, and J. D. Birchall, "A Simple Way to Make Tough Ceramics," Nature, 347[6292] 455 (1990).

67. D. Kovar, B. H. King, R. W. Trice, and J. W. Halloran, "Fibrous Monolithic Ceramics," Journal of the American Ceramic Society, 80[10] 2471-87 (1997).

68. D. R. Beeaff and G. E. Hilmas, "Rheological behavior of coextruded multilayer architectures," J Mater Sci, 37[6] 1259-64 (2002).

69. R. Bermejo, Y. Torres, A. J. Sánchez-Herencia, C. Baudín, M. Anglada, and L. Llanes, "Residual stresses, strength and toughness of laminates with different layer thickness ratios," Acta Materialia, 54[18] 4745-57 (2006).

VITA

Connor Charles Wittmaier was born on in St. Louis, MO. In August of 2011, Connor started his undergraduate degree in Ceramic Engineering at Missouri University of Science and Technology. During his undergraduate career, Connor joined several student groups including Keramos, Alpha Sigma Mu, and Material Advantage where he served as webmaster in the 2012-2013 academic year. During the following year, Connor worked as an undergraduate research assistant for Dr. Hilmas and Dr. Fahrenholtz in their ultra-high temperature group. Over the summer of 2014, Connor accepted a co-op with GE Aviation.

Connor stayed at Missouri S&T and began his graduate work for Dr. Fahrenholtz in January of 2015, working on advanced ceramics used in advanced structures. While performing this research Connor helped with the materials characterization and properties lab, gave presentations at several different conferences, and has written two papers. Connor received his M.S. degree in Ceramic Engineering from Missouri S&T in July of 2017, and will continue his career at the Missile Defense Agency in the Department of Defense.